A Reproduced Copy

OF

ngr-05-007-091

NUMERICAL SIMULATION OF WEATHER AND CLIMATE

Technical Report No. 4

NUMERICAL SIMULATION OF THE 1970-71 EOLE EXPERIMENT

by

Fedor Mesinger and Yale Mintz

15 January 1970

Sent for PCF

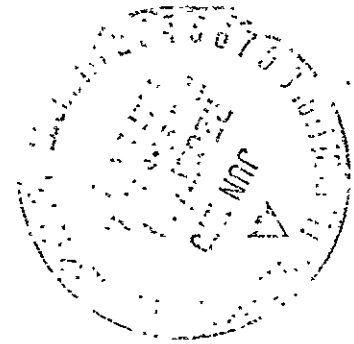

Department of Meteorology

University of California, Los Angeles

NUMERICAL SIMULATION OF WEATHER AND CLIMATE

Technical Report No. 4

NUMERICAL SIMULATION OF THE 1970-71 EOLE EXPERIMENT

by

Fedor Mesinger and Yale Mintz

15 January 1970

Department of Meteorology

University of California, Los Angeles

TABLE OF CONTENTS

1. INTRODUCTION

The planning of the First GARP Global Experiment includes a subsystem of superpressure balloons (WMO-ICSU, 1969, p. 10). Earth orbiting satellites will track the motions of these balloons, and communicate with sensors on them, and thereby provide observations of the wind, temperature, pressure and geopotential of the air at the position of each balloon (cf. Lally and Lichfield, 1969; Morel, 1969).

A preliminary test of a satellite-balloon system of this kind, on a hemispheric-scale, is the "Eole Experiment", sponsored by the French Centre National des Etudes Spatiales in cooperation with the Planetary Radiations Branch of the Laboratory for Atmospheric and Biological Sciences of the U.S. National Aeronautics and Space Administration.

The Eole Experiment is scheduled for the Southern Hemisphere summer of 1970-71. According to the present plans, after the tracking and interrogation satellite has been placed in its polar orbit, 10 balloons will be released per day at each of the following launching sites in Argentina:

A. Lago Fagnano	54.5°S	67.5°W,
B. Neuquén	38.6°S	68.1°W,
C. Mendoza	32.5°S	68.5°W,

until a total of 500 balloons are in the air. These balloons will float on the surface of constant air density, which in the Standard Atmosphere has the pressure of 200 mb. The balloons are expected to have a 90 day mean lifetime. As individual balloons fail, the total number of 500 balloons will be maintained in the air by additional launchings, until all of the 750 balloons provided for the experiment have been used. Any balloon will be automatically cut down if it crosses into the Northern Hemisphere.

In the study presented in this report, we have attempted to anticipate the performance of the Eole system by simulating the trajectories of the balloons for a 130 day period. For this prupose we use the winds produced in a numerical simulation of the general circulation of the global atmosphere.

2. NUMERICAL SIMULATION OF THE GLOBAL WIND FIELD

The winds used in this study were obtained by numerical integration of the primitive equations with a two-level version of the general circulation model described by Arakawa, Mintz and Katayama (1970). In this model, the atmosphere between the earth's surface and 200 mb pressure is divided into two layers of equal mass. The time-dependent variables are the horizontal velocities and temperatures in the middle of the two layers, the surface pressure, the water vapor in the lower layer, and the water stored in the ground. The earth's surface is specified as open ocean, ice covered ocean, and bare land or snow covered land. The height of the land follows the large scale mountain systems. The temperature of the ocean surface and the distribution of the sea ice are prescribed as their observed annual mean values.

The grid points are at every 5° of longitude and 4° of latitude, from pole to pole. The finite space-difference scheme maintains the integral constraints of physical importance, and the scheme suppresses any computational noise in the pressure and temperature fields which is not under control of the geostrophic adjustment process. The time step is 6 minutes, using a combination of the Heun and the Matsuno time-difference schemes.

Kinetic energy dissipation in the model is only by surface friction and friction due to the vertical eddy stress between the two wind levels. The heating by absorption of solar radiation depends on the calculated water vapor and diagnostically determined clouds. The long wave radiative cooling depends on the water vapor and clouds and on the temperatures of the air and earth's surface. The sensible heat transfer, at the air-ground interface, depends on the temperature difference between the air and the ground. Over bare land and over snow and ice surfaces, the ground temperature is calculated from the surface energy budget. Latent heat release is obtained from the calculated precipation.

There are two kinds of precipitation in the model. One is large scale, which occurs when the lapse rate is absolutely stable and the grid scale humidity exceeds its saturation value. The other kind is cumulus-convective precipitation. The cumulus-convection is of three forms: low-level, middle-level and penetrative convection, depending on the humidity and the vertical distribution of temperature. The low-level convection only transfers sensible heat and water vapor from the ground to the air. It forms low level convective clouds which influence the short and long-wave radiative transfers, but all the water in these clouds evaporates into the air. The middle-level and penetrative convection not only transfer heat and water vapor, but also release latent heat of condensation.

Evaporation from the surface depends on the wind speed and on the difference between the vapor pressure of the air and the vapor pressure of the surface. For open ocean, ice and snow, the surface vapor pressure is its saturation value. For bare land, the surface vapor pressure depends on the wetness of the ground. The ground wetness is calculated from the precipitation, evaporation and runoff.

he initial state in this numerical simulation of the global atmospheric circulation, was a state of zero winds (atmosphere and earth in solid rotation);

three-dimensional isothermalcy, at 250°K; a constant sea level pressure, of one atmosphere; no water-vapor in the air; and dry ground.

The wind and mass fields used to calculate the balloon trajectories in this numerical simulation of the Eole Experiment, are from the 130 day period, day 341 to day 471 of the numerical integration, during which time the sun changed its declination and distance from that of 1 December to 11 April.

3. CALCULATION OF BALLOON TRAJECTORIES

In the numerical simulation; we calculate the trajectories of the balloons which float on the surface of constant air density, $\rho_2 = 0.329$ kg/m^3, which is the air density at 200 mb in the Standard Atmosphere.

From the two levels at which the winds and temperatures are computed in the model, the wind components are extrapolated linearly with pressure to the density surface, ρ_2, where they are used to transport the balloons.

Although the time-dependent fields in the numerical simulation of the global circulation were calculated in 6 minute steps, for practical reasons these fields were recorded on magnetic tapes only at 6 hour intervals. For the balloon trajectory calculations the 6 hourly winds were linearly interpolated to 1.2 hour intervals.

Horizontal interpolation, from the grid points at which the winds were computed (every 5° of longitude and 4° of latitude) to the locations required for the trajectory calculation, was by linear interpolation in longitude and latitude.

After the winds were interpolated vertically, in time, and horizontally, to the locations of every balloon, 1.2 hour forward displacements were taken along the great circle paths given by the interpolated winds. At the endpoint positions of the 1.2 hour displacements, the time and space interpolations of the wind were repeated, and new 1.2 hour forward displacements calculated. The end points of these second displacements were then connected to the starting points of the initial displacements by great circle segments, and the median points of these segments were taken as the positions of the balloons at the end of the first 1.2 hour time step. This space- and time-centered procedure for computing trajectories on a spherical surface corresponds to the method given by Henrici (1962) for calculations on a plane, with his equation 3-47 and the constant, $\alpha = 0.5$.

Iteration of the above procedure in 1.2 hourly steps, for the 500 balloons, and for 130 days, produced the distribution of balloons shown in the next section.

In the numerical simulation, the balloons were introduced directly on the density surface, ρ_2, at intervals of 2.4 hours, at the location of each of the three launching stations, until 500 balloons were in the air. The first three balloons were introduced at time 0.0 GMT, December 1, year 1, in the model atmosphere; and the last two balloons at 14.4 GMT, December 17, year 1. The balloons are identified by the letters A,B,C according to their launch sites: A = Lago Fagnano; B=Neuquén; and C=Mendoza.

4. HEMISPHERIC MAPS OF THE BALLOON DISTRIBUTIONS

The calculated distributions of the balloons are shown, in figures through 28, on polar equal area maps of the Southern Hemisphere. Because the positioning of the balloons is constrained in the figures by the resolution of the line-printer, wherever two balloons fall within the same printing location the second balloon (and, more rarely, others too) is printed in the nearest vacant printing space at one or the other side, or below, the true printing location.

On day 0 (hour 0.0), there are only three balloons shown on the maps, one at each of the three launch sites.

At day 2.5 there are 78 balloons in the air, and they show westerly steakline waves, of variable amplitudes.

At day 5 there are 153 balloons, and the streaklines are still relatively well defined by balloons B and C. But balloons A, those launched at Lago Fagnano, have mostly separated into two loose clusters.

By day 10 balloons B and C form a ring around the globe, with about 7 small amplitude waves in the streaklines. Some of the balloons A are now in the polar region. By this time, 303 balloons are in the air.

On day 15 there are 453 balloons in the air. But there are now fewer balloons in the polar region.

By day 20, 500 balloons are in the air. These same balloons remain in the air for the remainder of the 130 days, as we do not simulate any balloon failures and replacements.

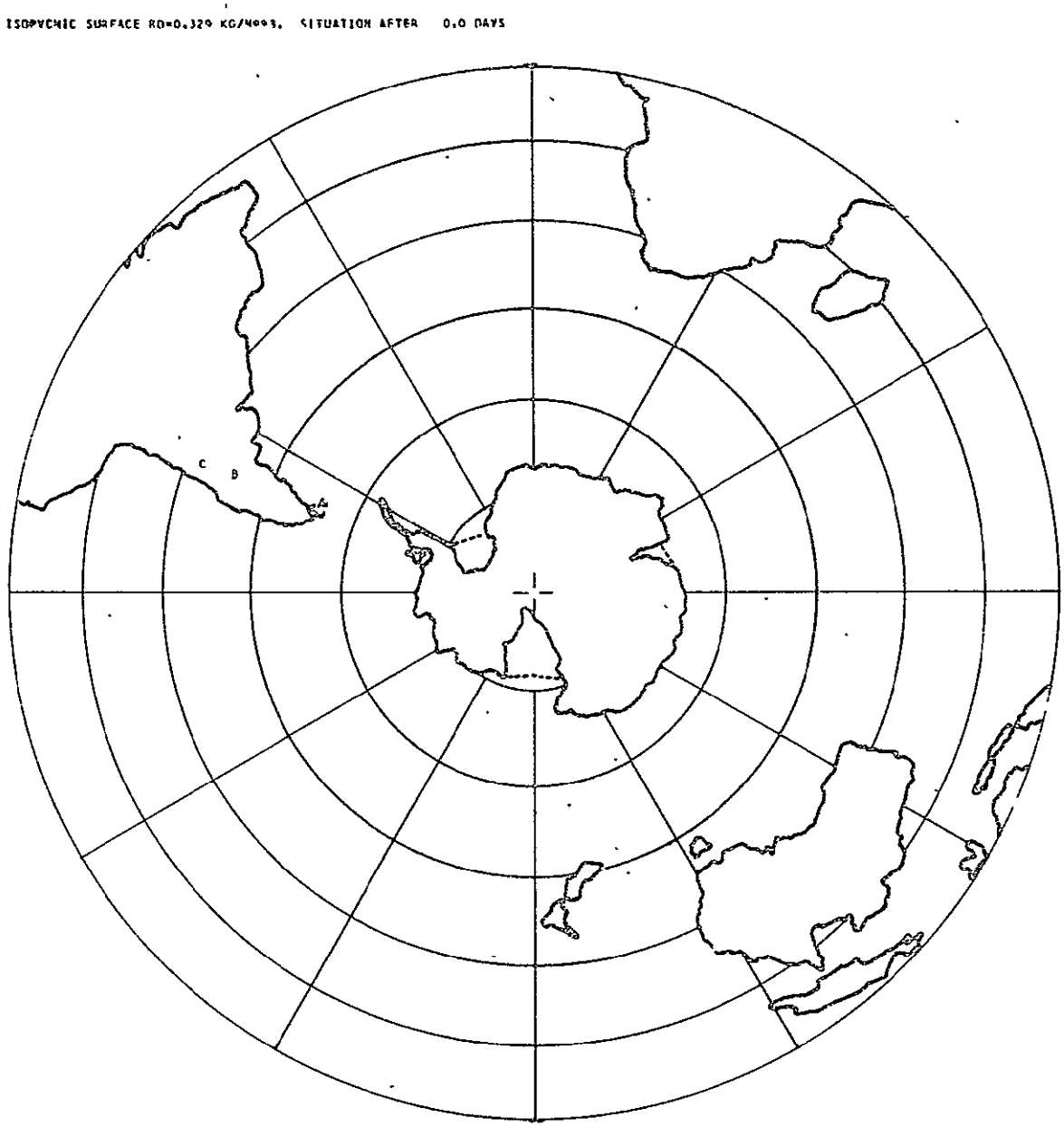

Fig. 1. Balloon positions, on a polar equal area projection, at day 0.0.

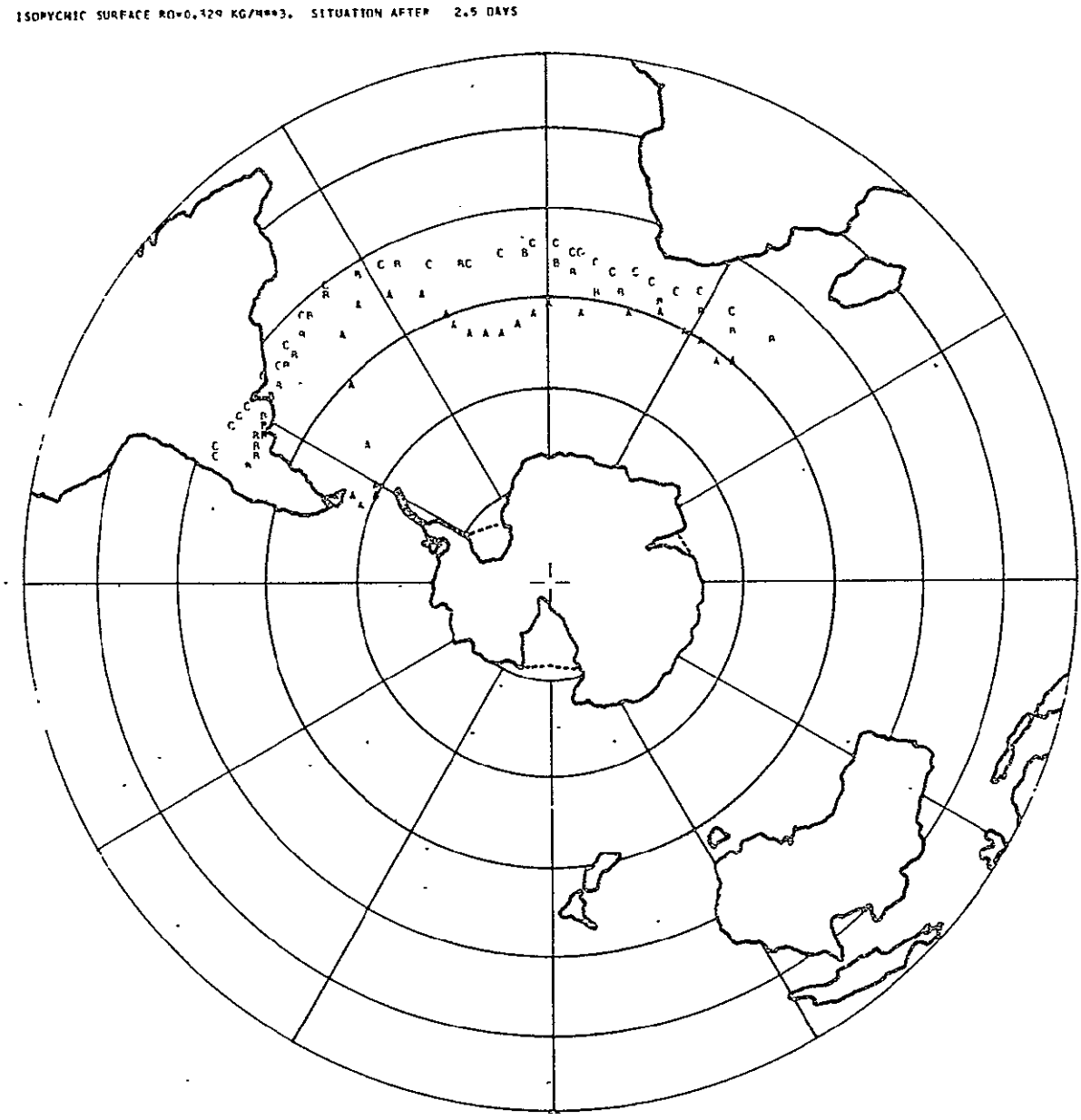

Fig. 2. Balloon positions, on a polar equal area projection, at day 2.5.

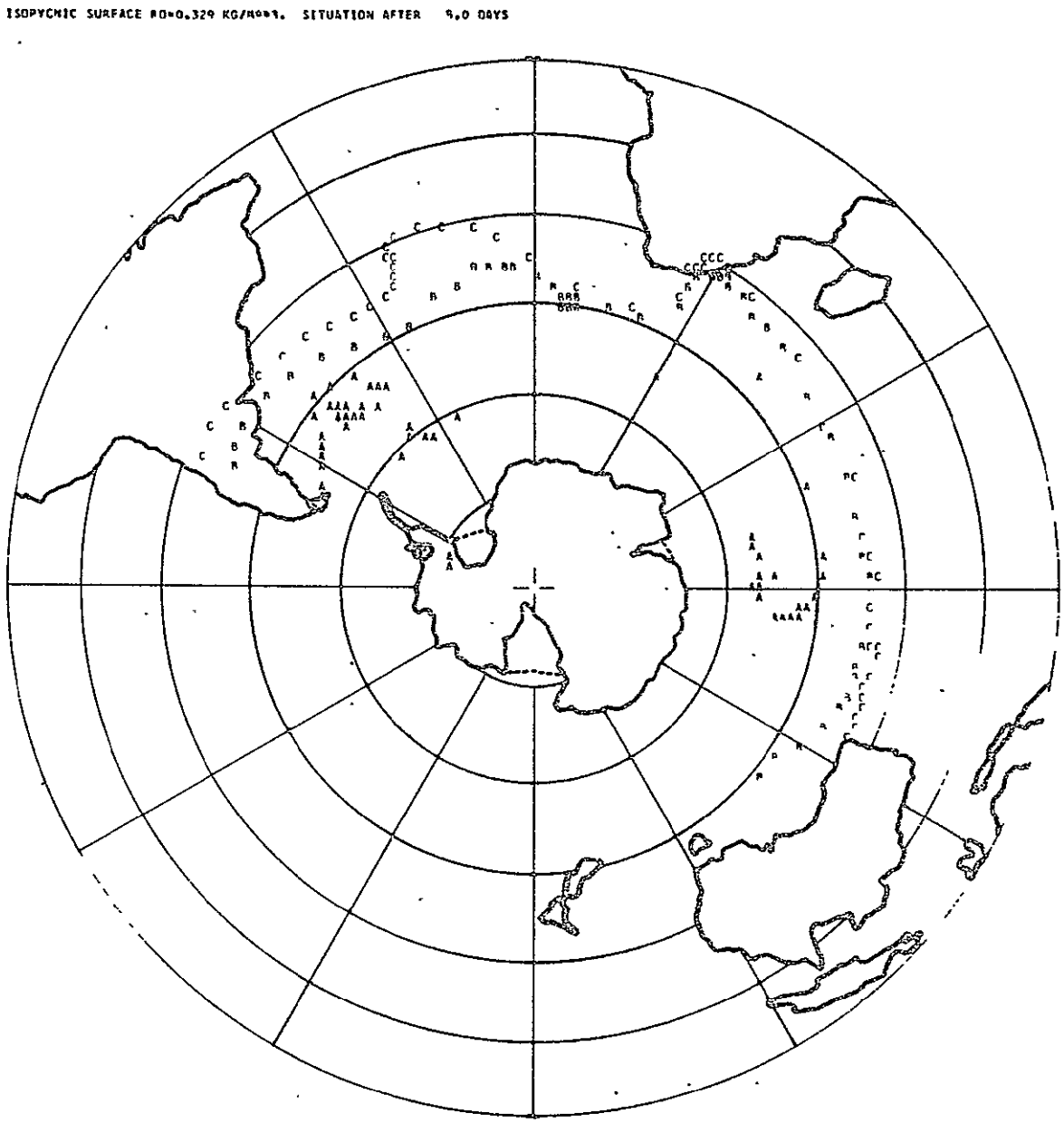

Fig. 3. Balloon positions, on a polar equal area projection, at day 5.

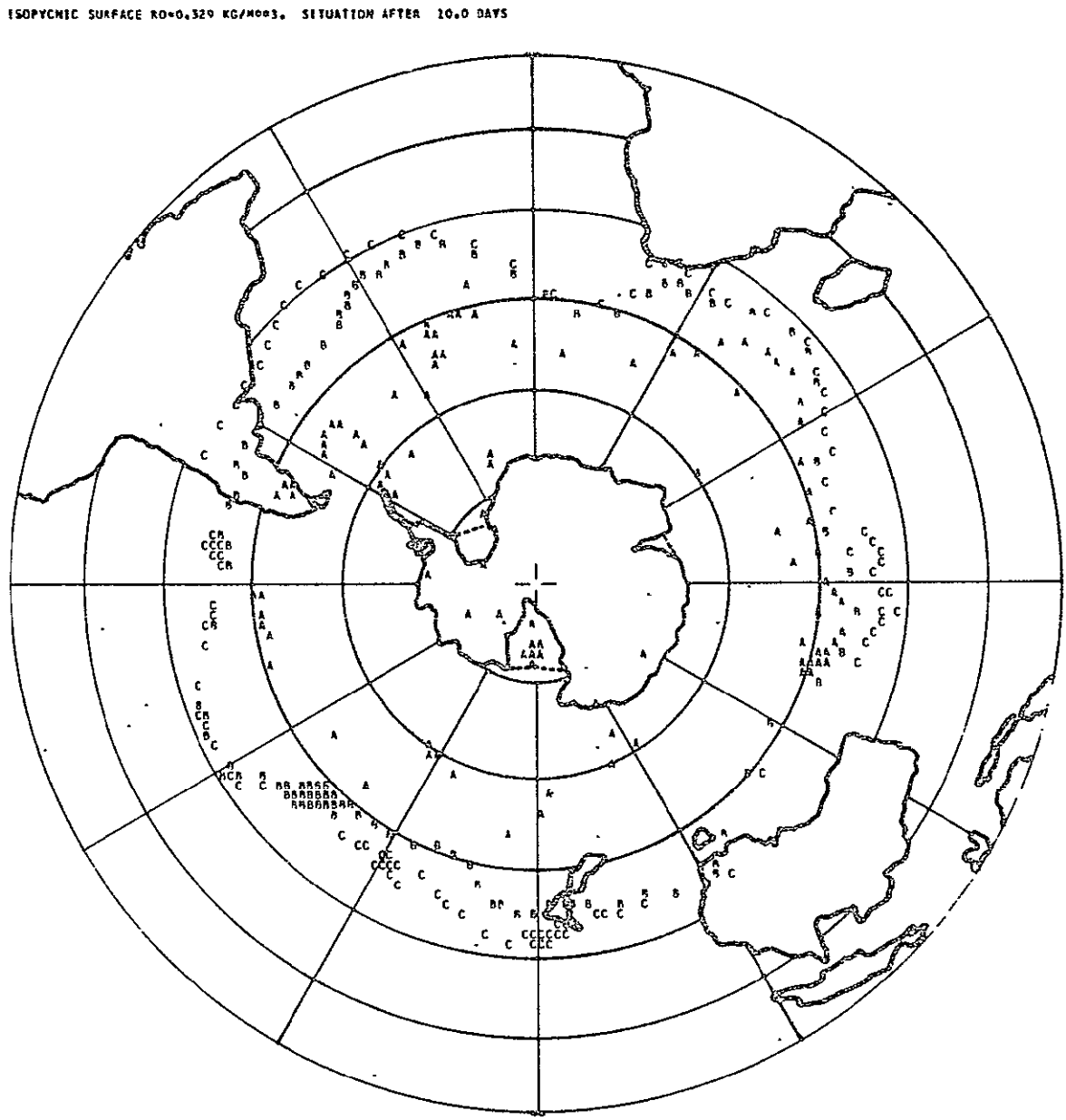

Fig. 4. Balloon positions, on a polar equal area projection, at day 10.

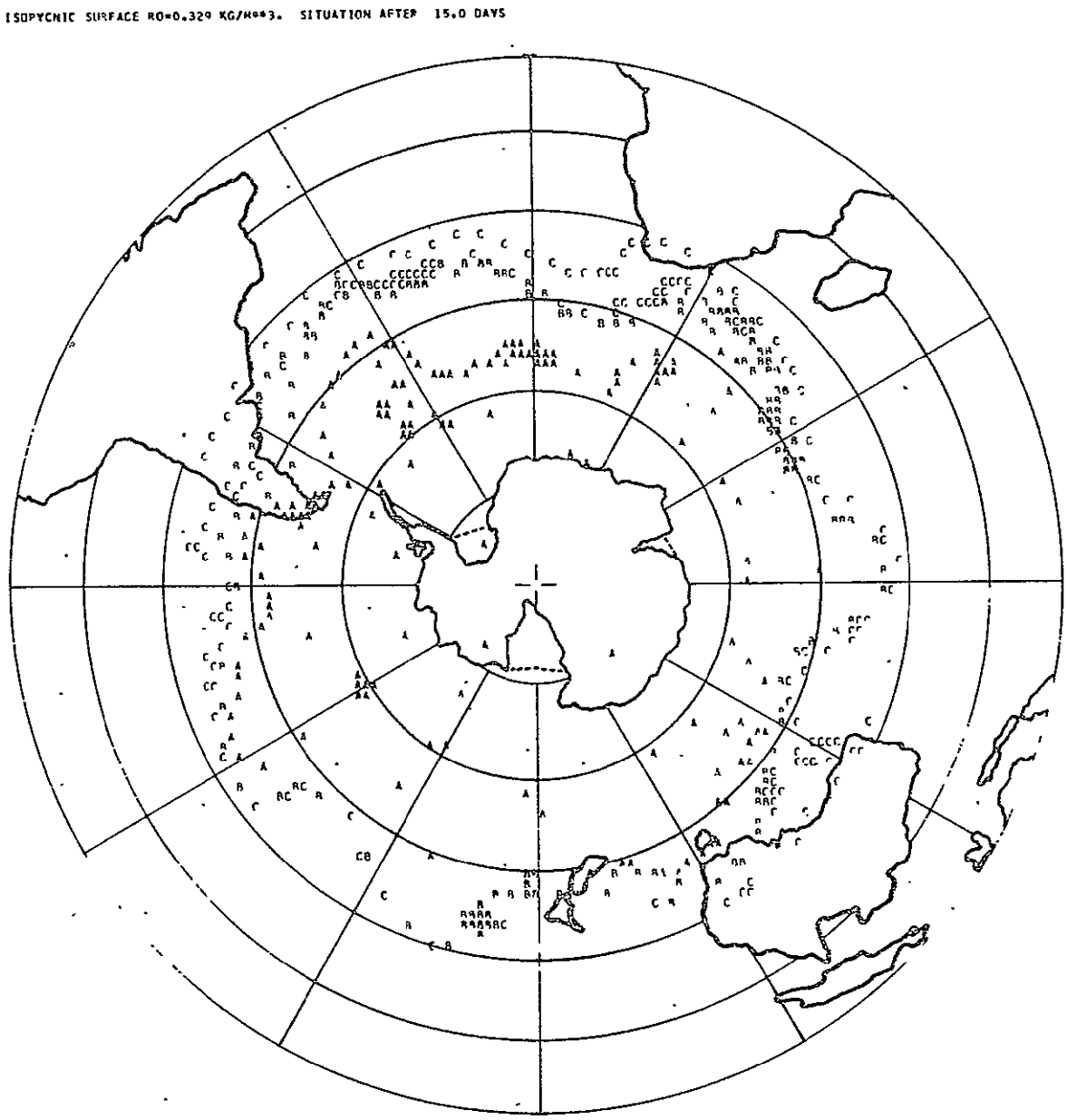

Fig. 5. Balloon positions, on a polar equal area projection, at day 15.

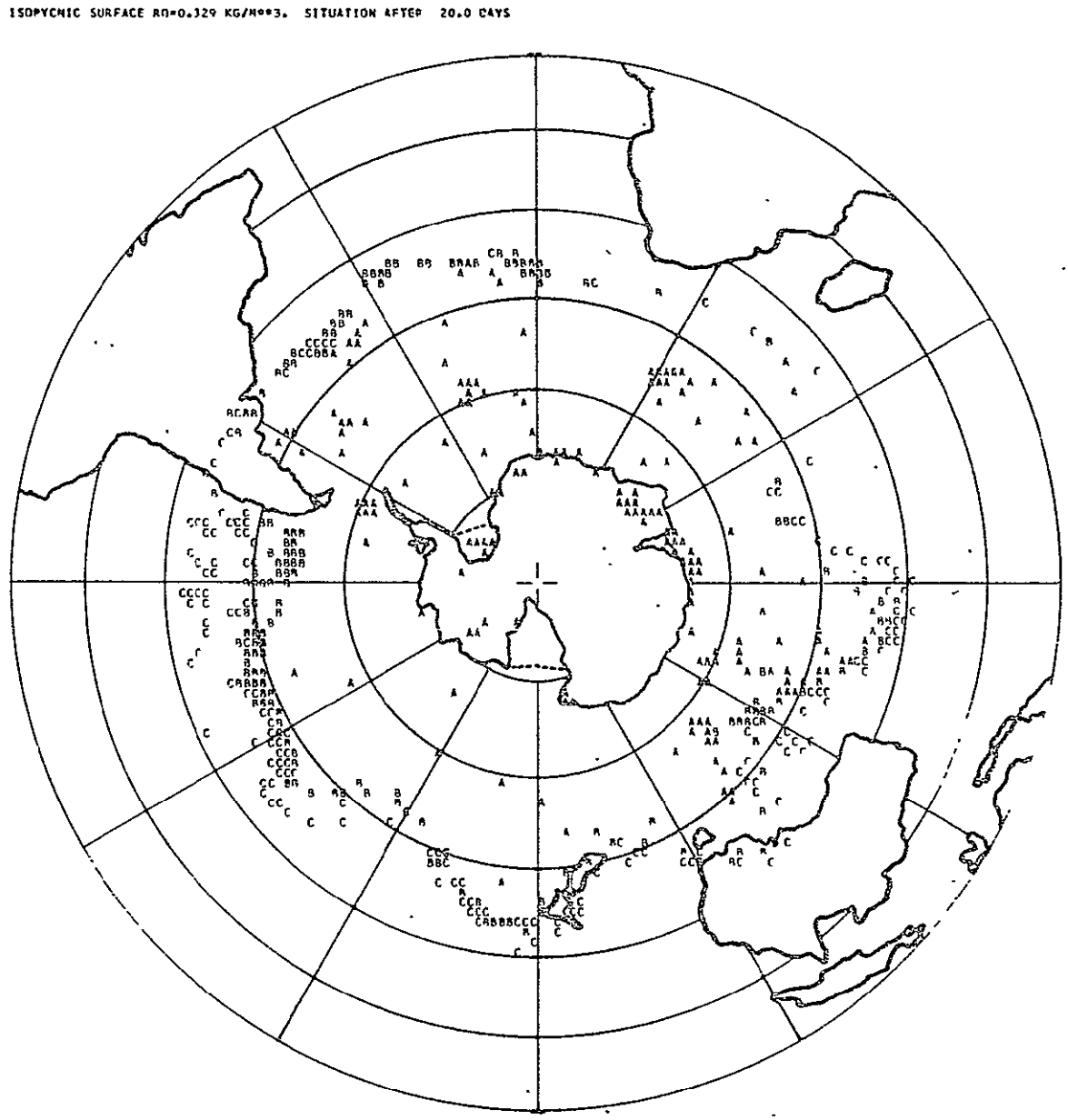

Fig. 6. Balloon positions, on a polar equal area projection, at day 20.

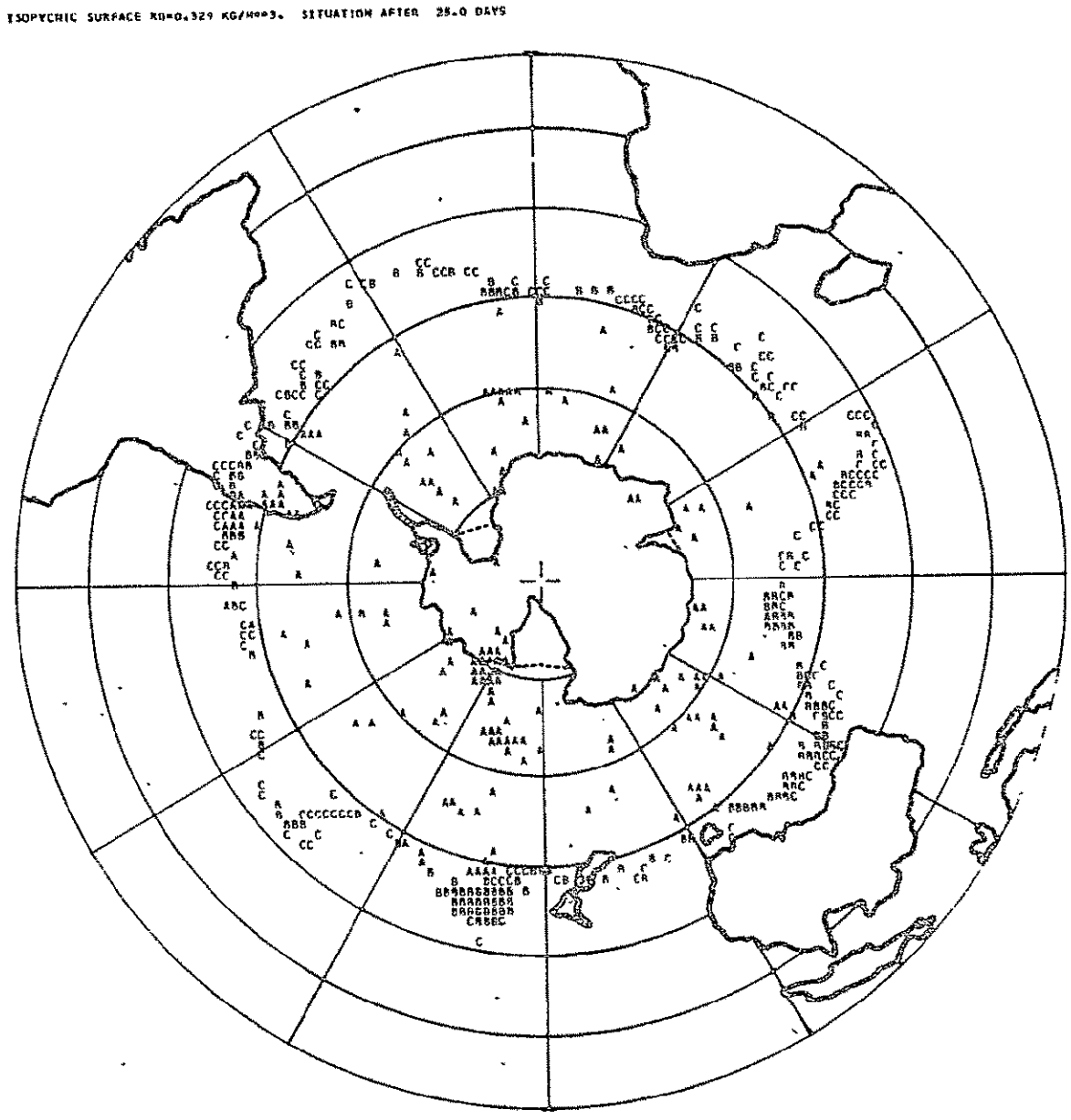

Fig. 7. Balloon positions, on a polar equal area projection, at day 25.

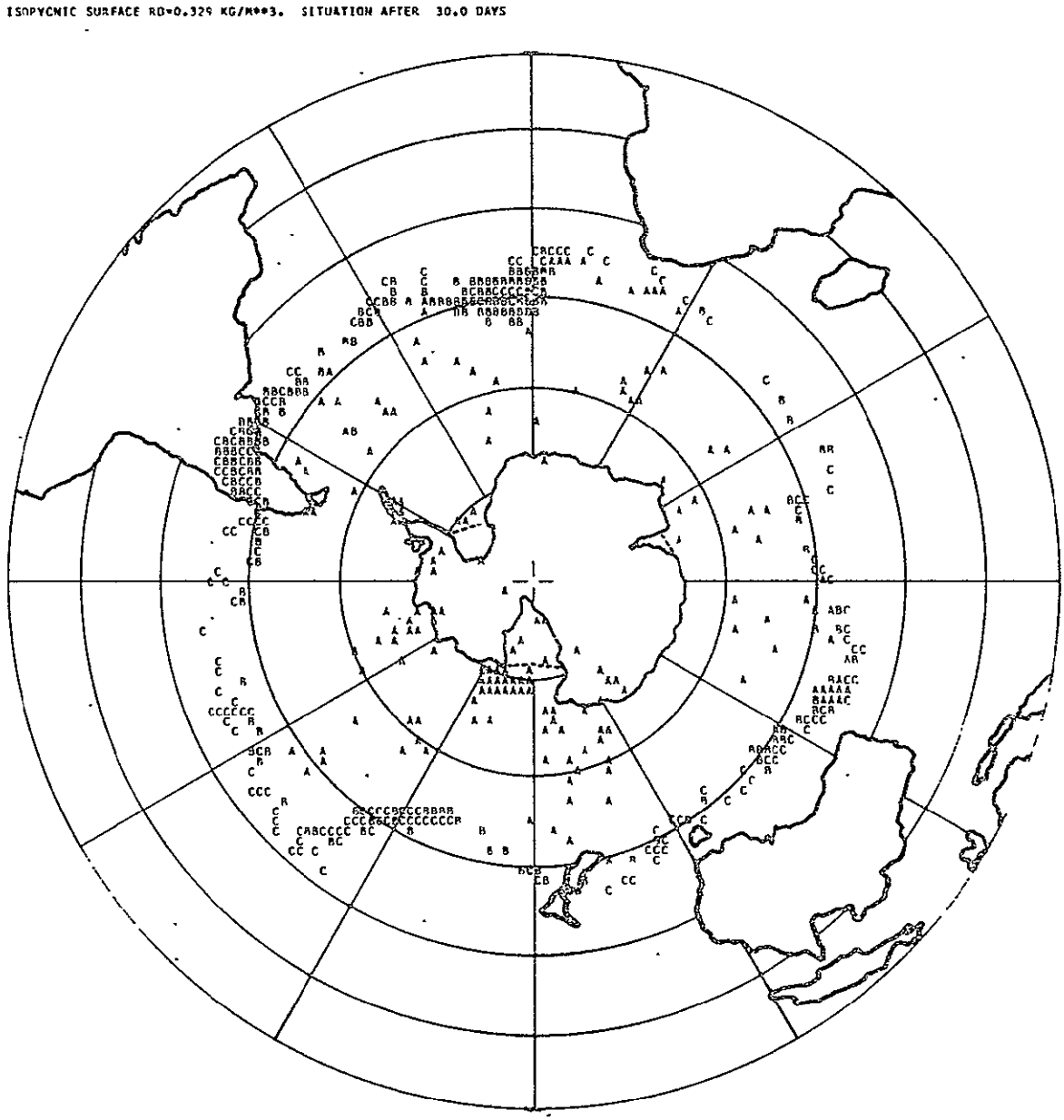

Fig. 8. Balloon positions, on a polar equal area projection, at day 30.

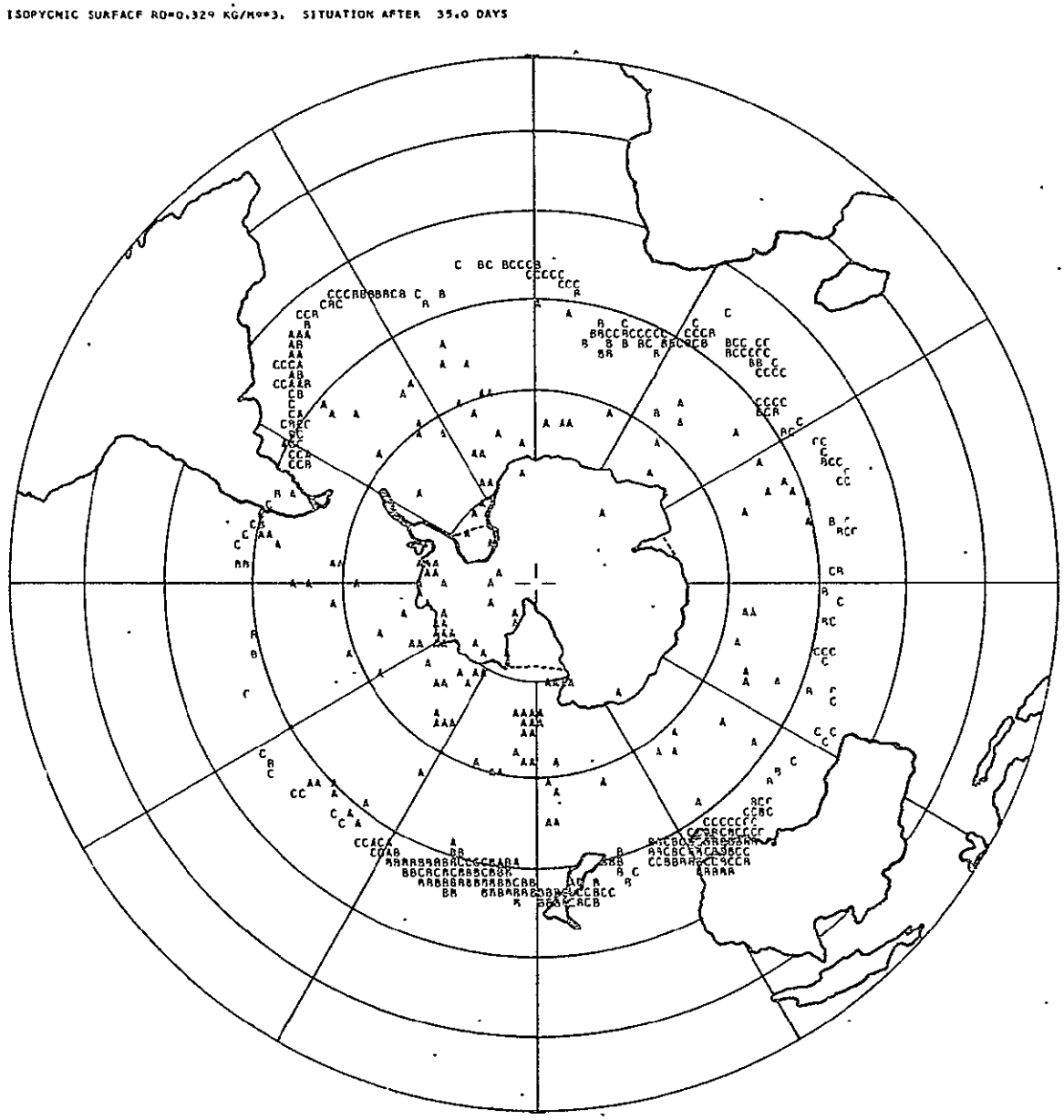

Fig. 9. Balloon positions, on a polar equal area projection, at day 35.

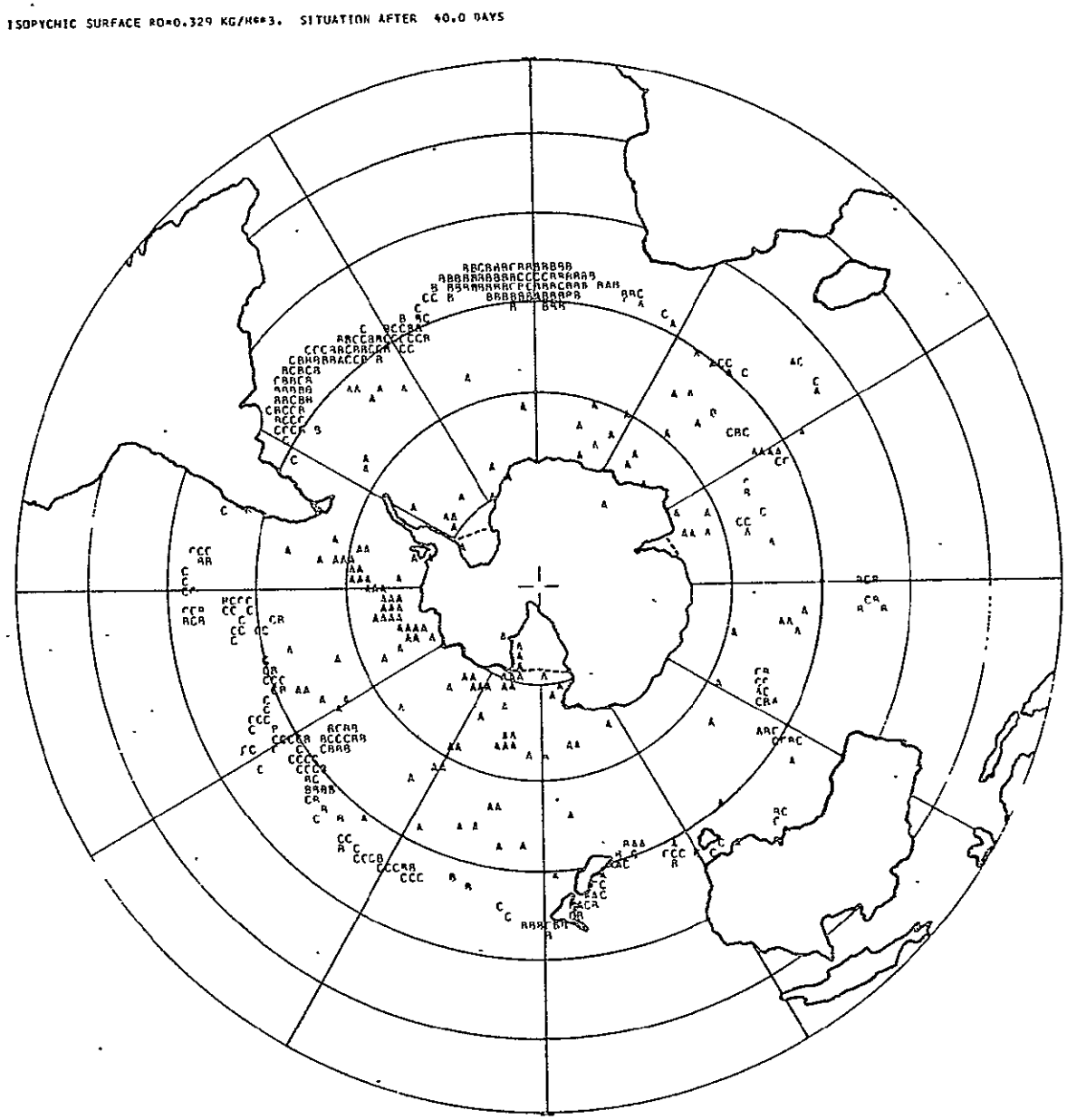

Fig. 10. Balloon positions, on a polar equal-area projection, at day 40.

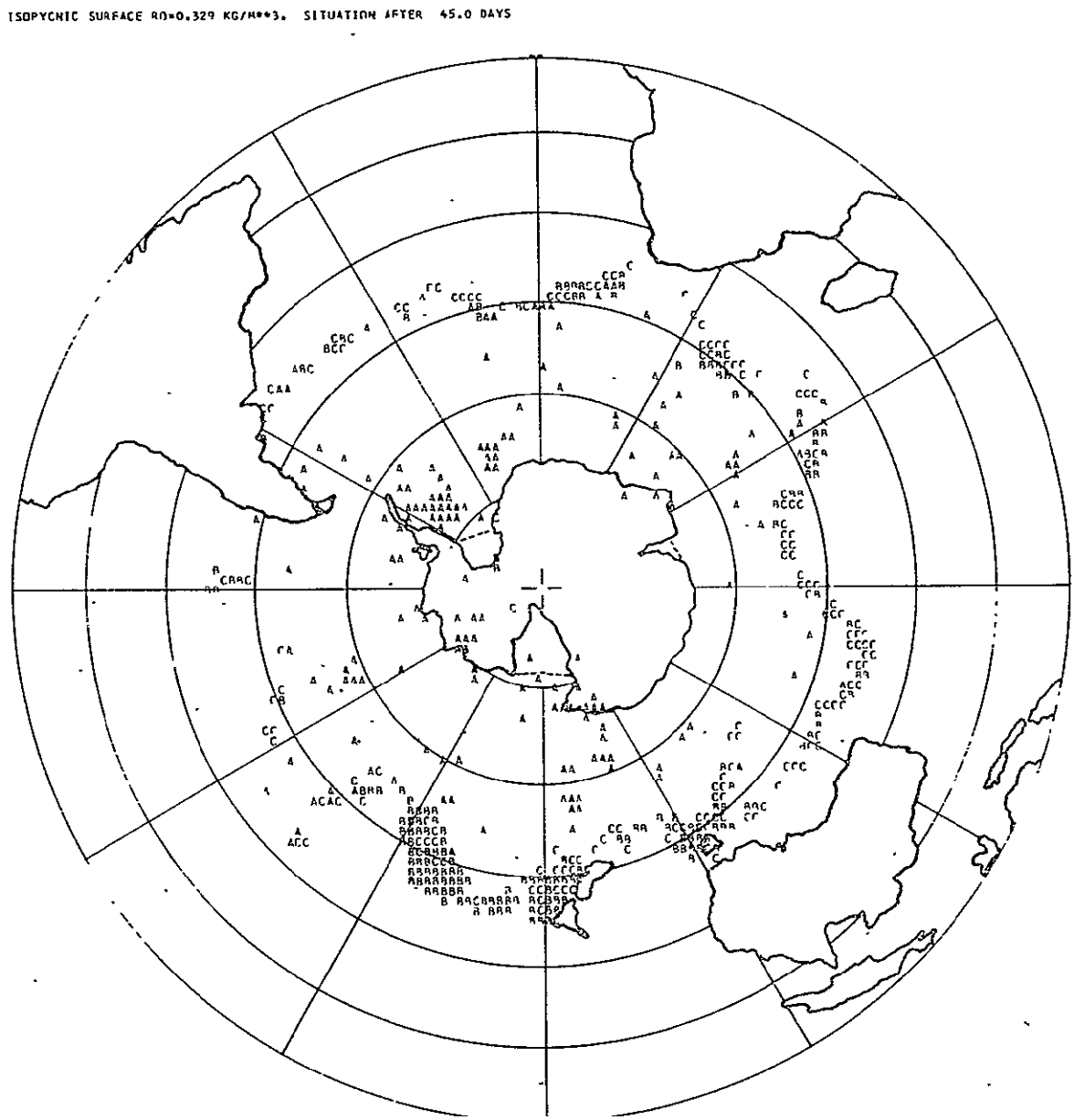

Fig. 11. Balloon positions, on a polar equation area projection, at day 45.

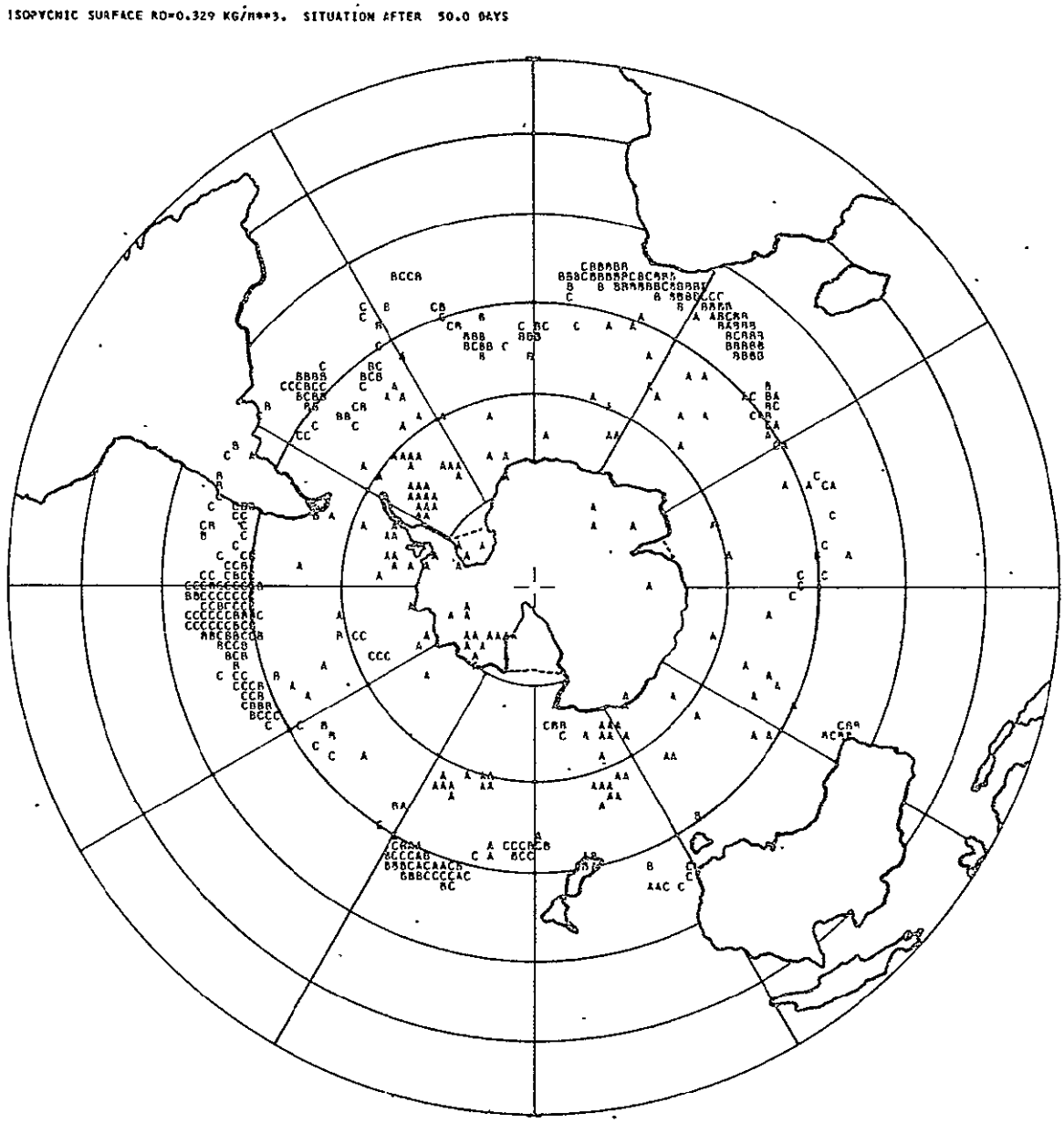

Fig. 12. Balloon positions, on a polar equal area projection, at day 50.

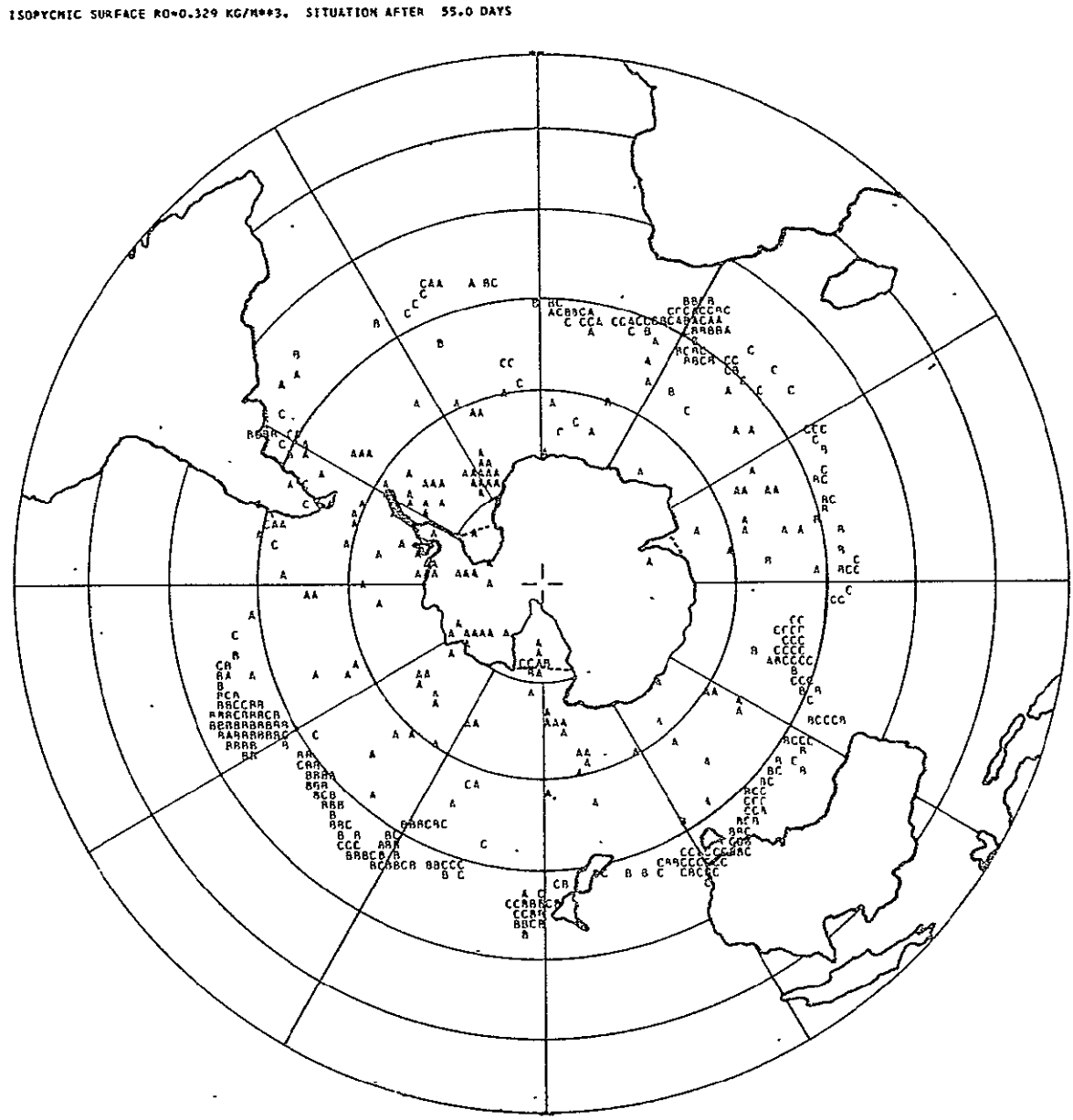

Fig. 13. Balloon positions, on a polar equal area projection, at day 55.

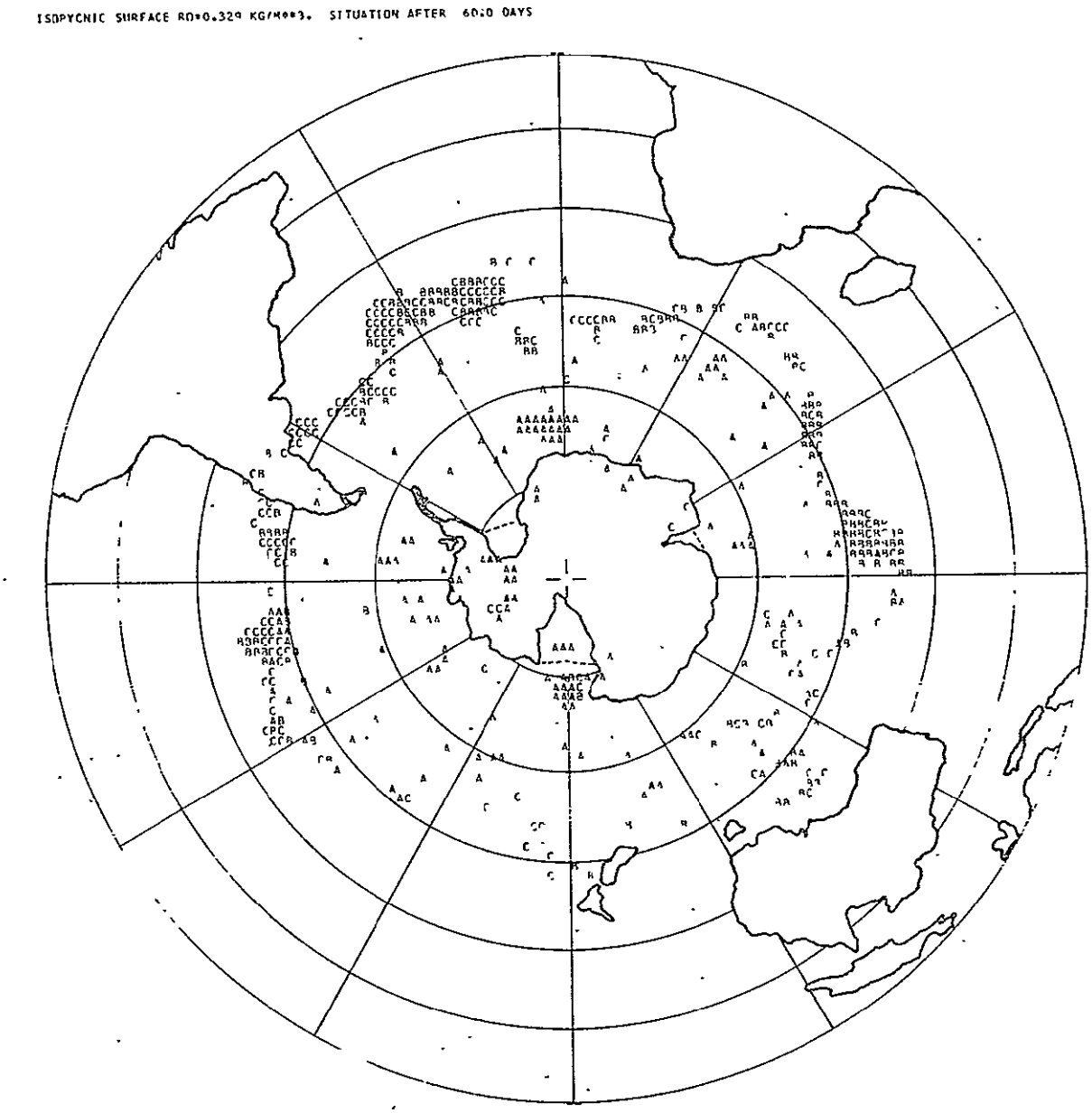

Fig. 14. Balloon positions, on a polar equal area projection, at day 60.

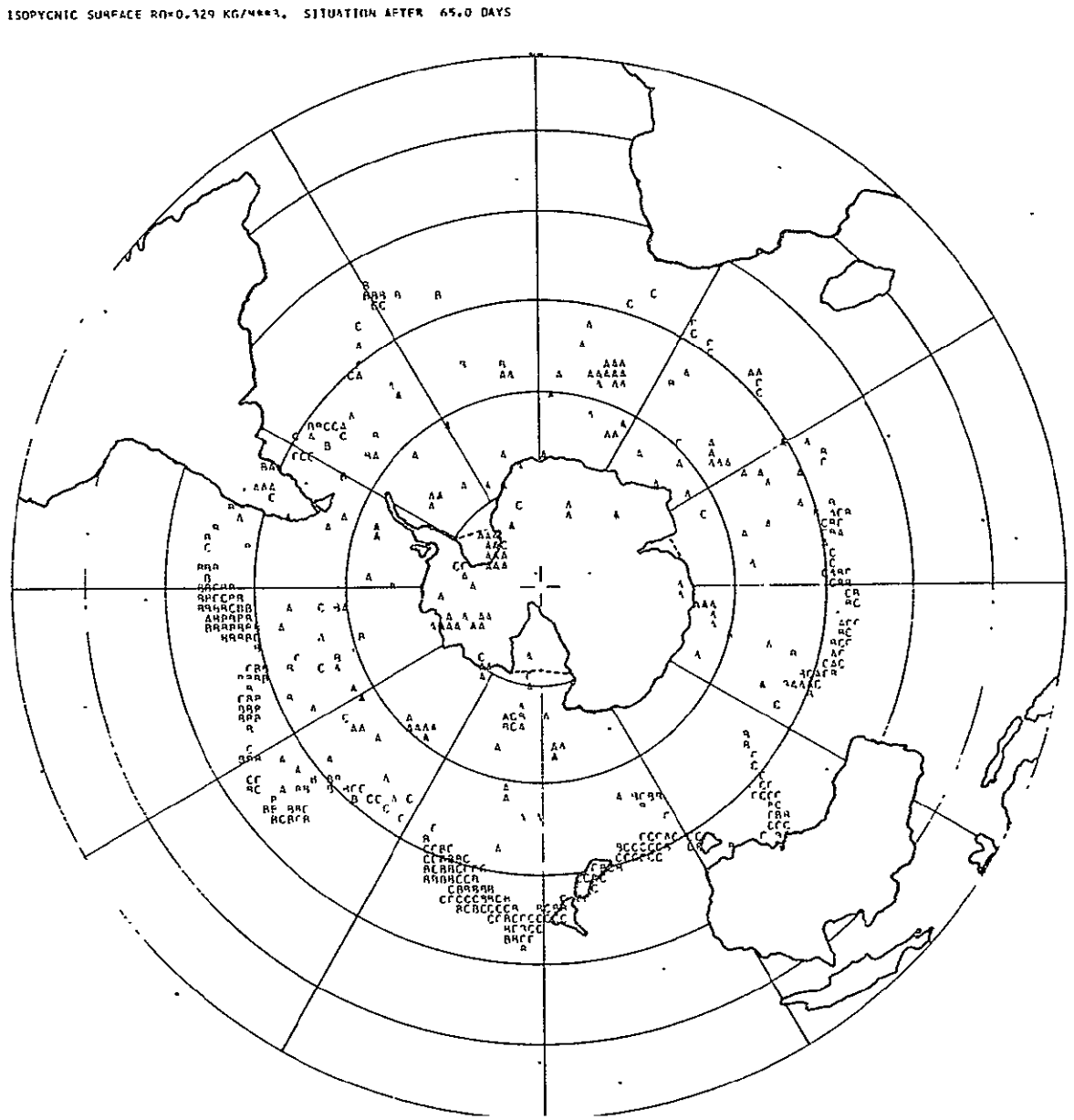

Fig. 15. Balloon positions, on a polar equal area projection, at day 65.

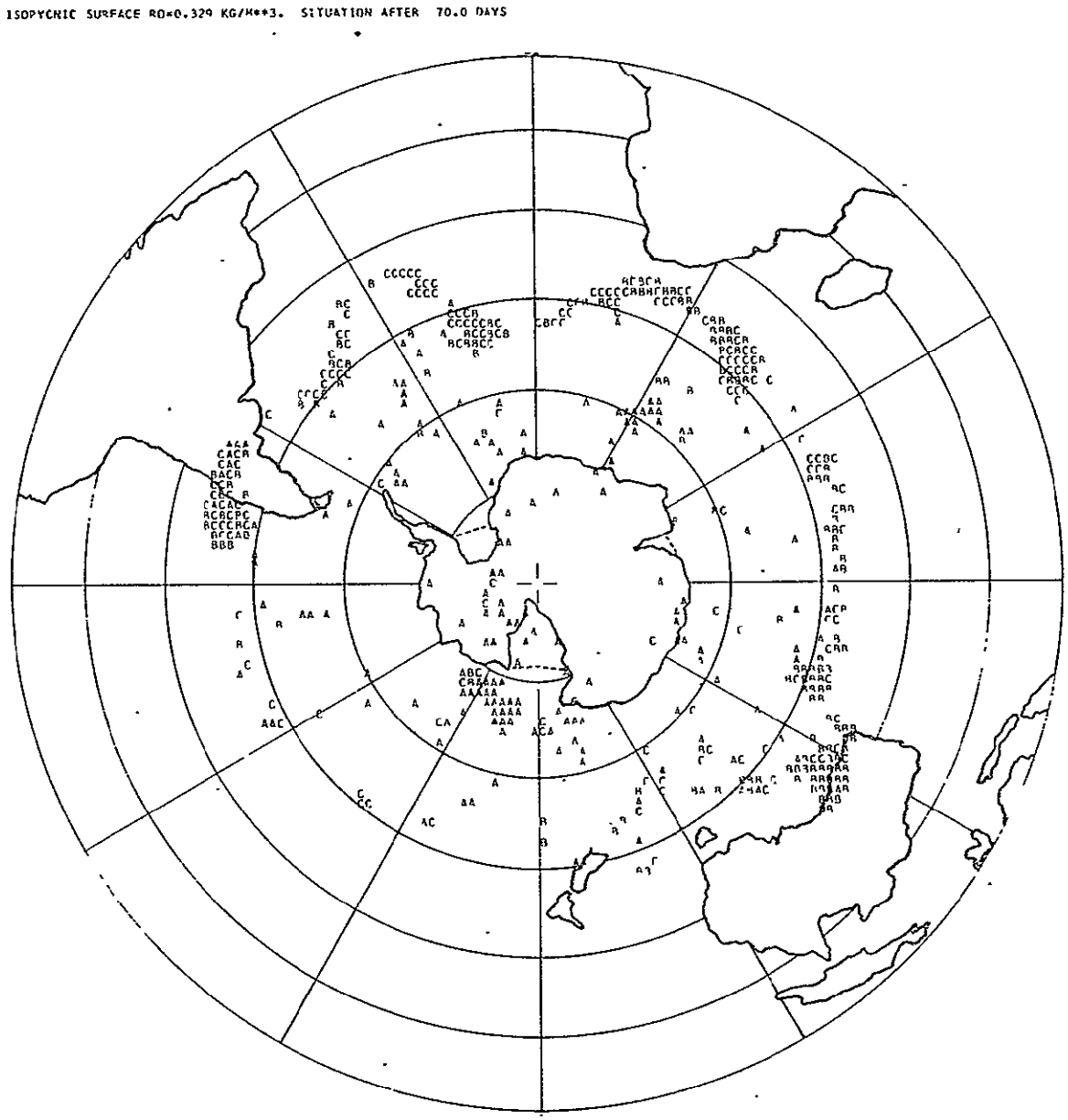

Fig. 16. Balloon positions, on a polar equal area projection, at day 70.

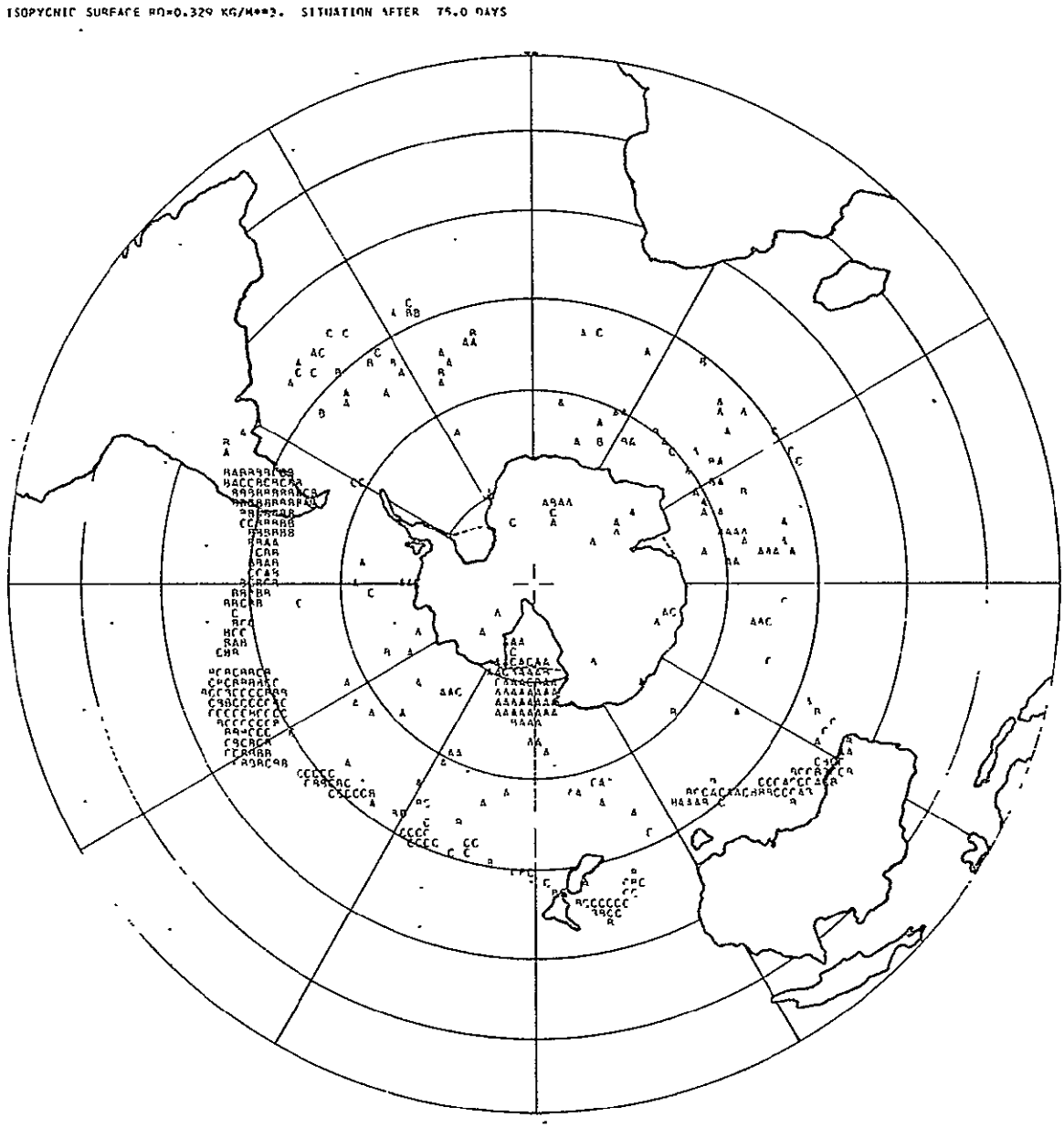

Fig. 17. Balloon positions, on a polar equal area projection, at day 75.

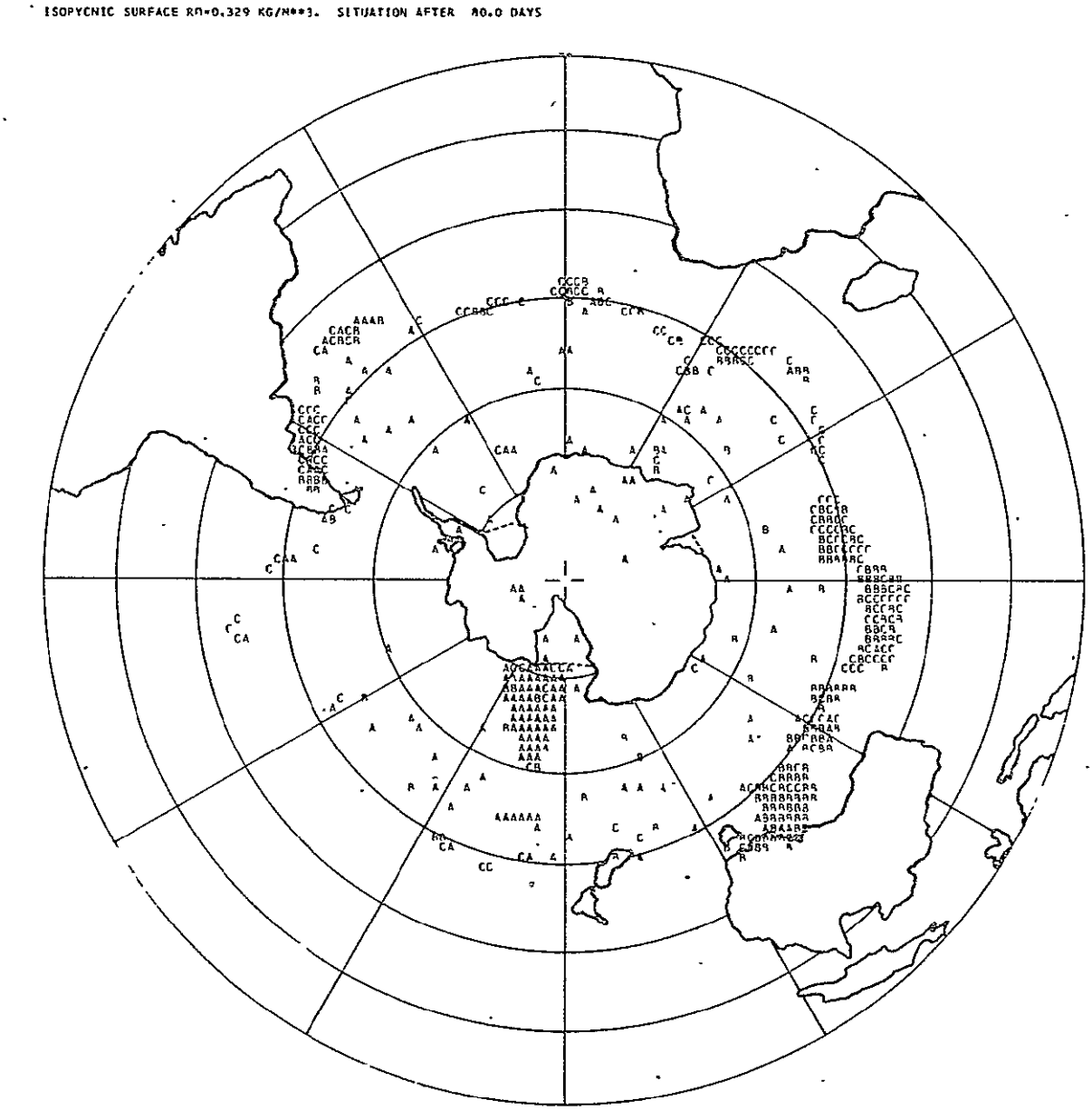

Fig. 18. Balloon positions, on a polar equal area projection, at day 80.

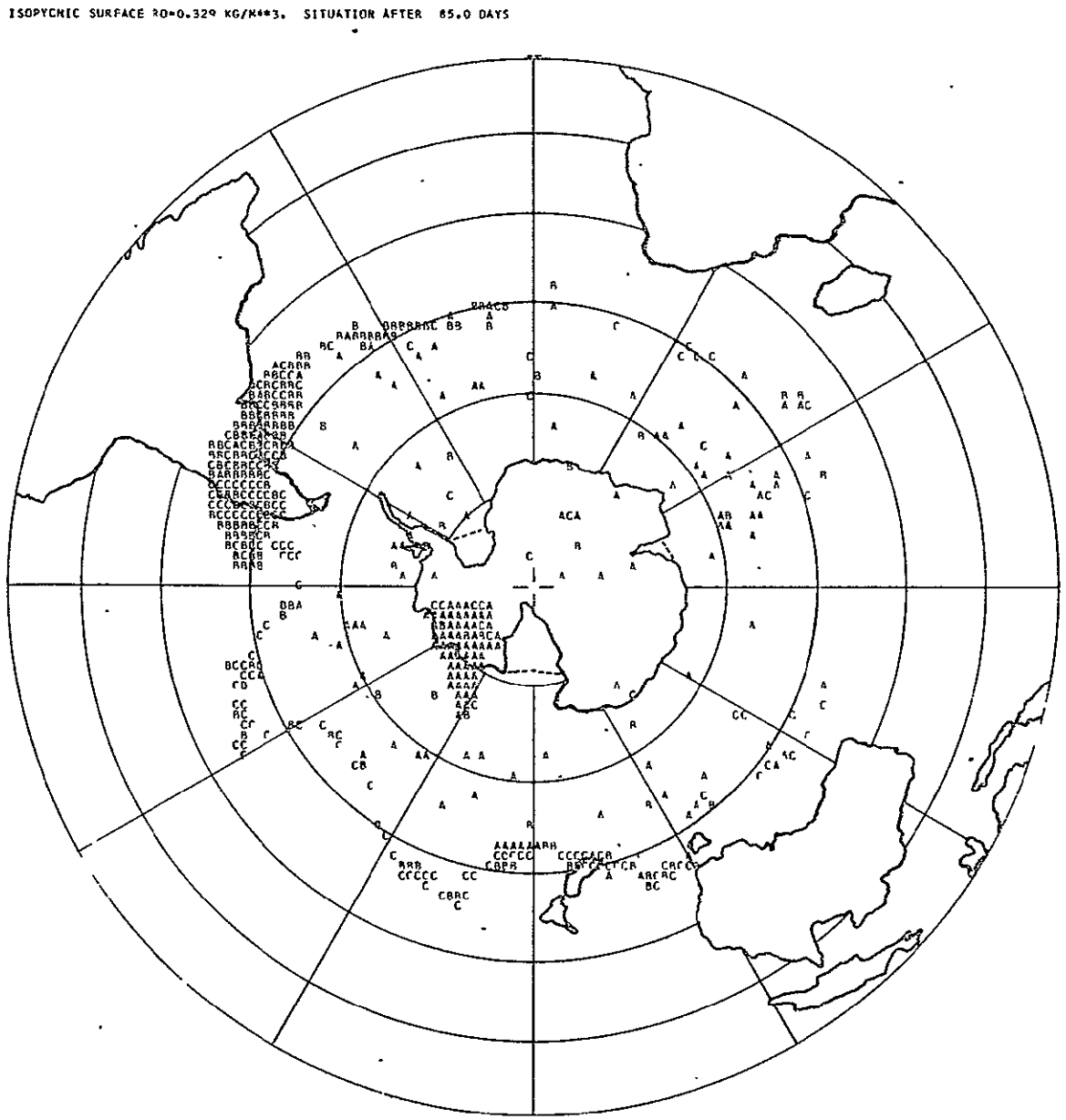

Fig. 19. Balloon positions, on a polar equal area projection, at day 85.

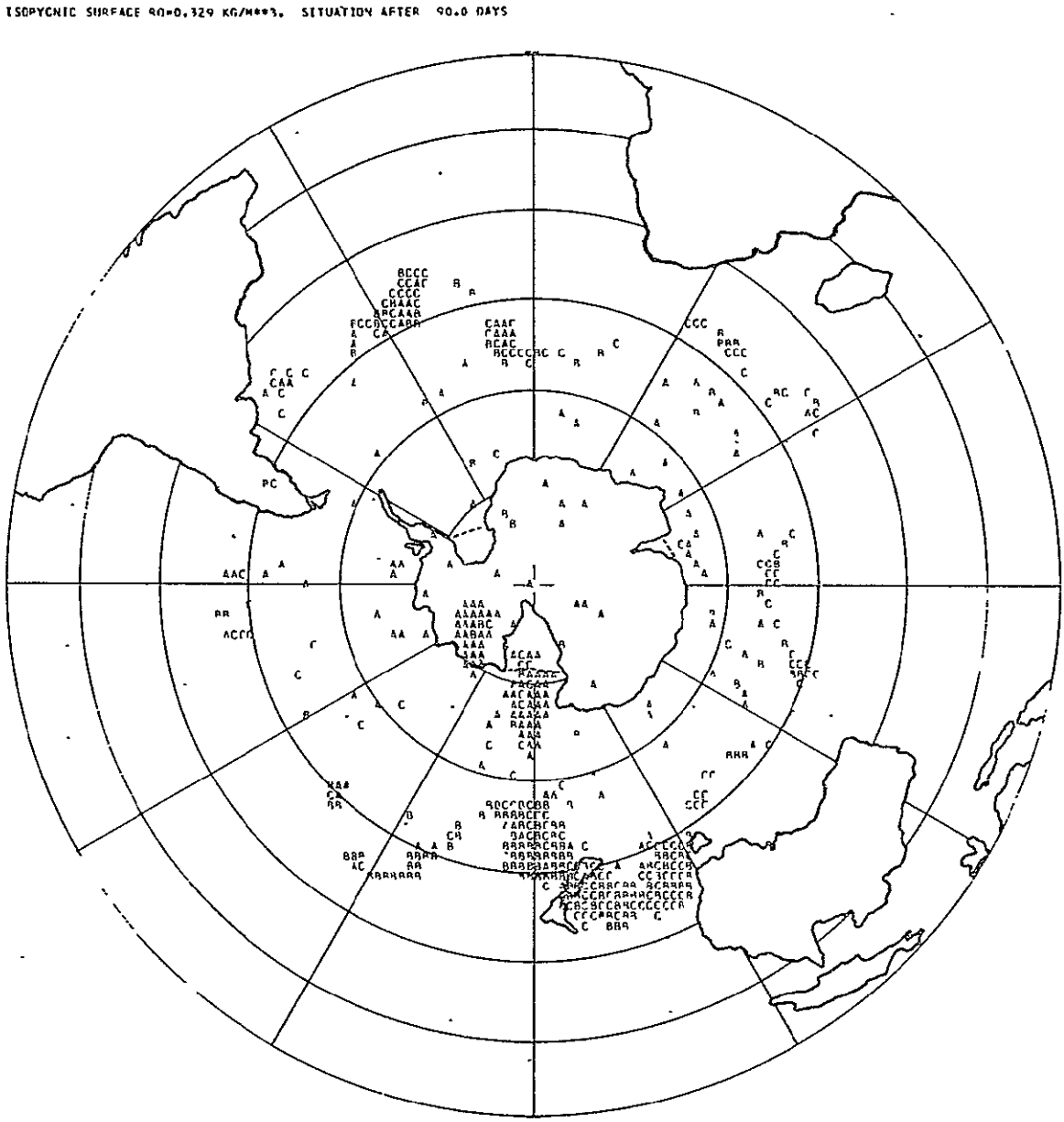

Fig. 20. Balloon positions, on a plar equal area projection, at day 90.

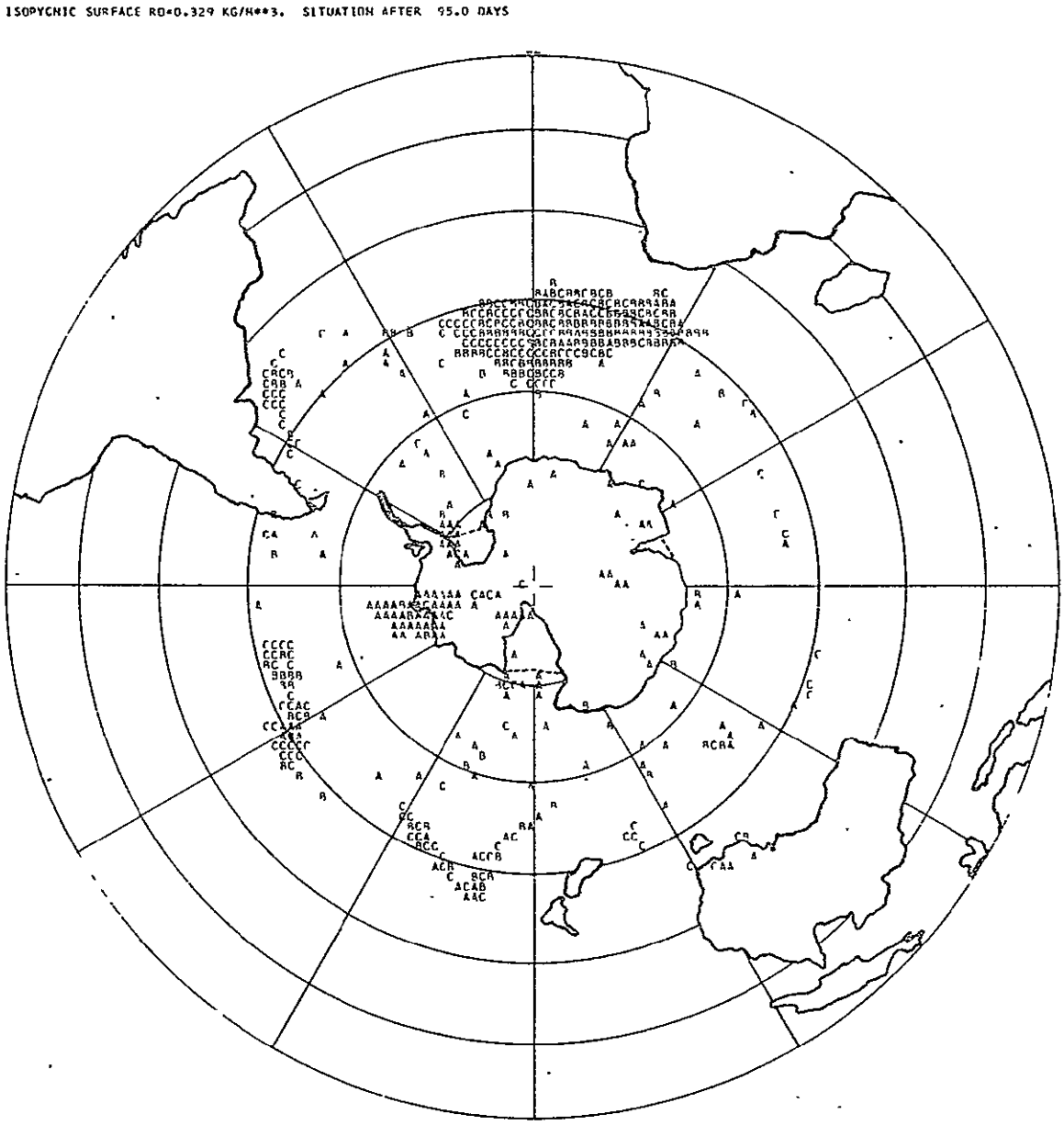

Fig. 21. Balloon positions, on a polar equal area projection, at day 95.

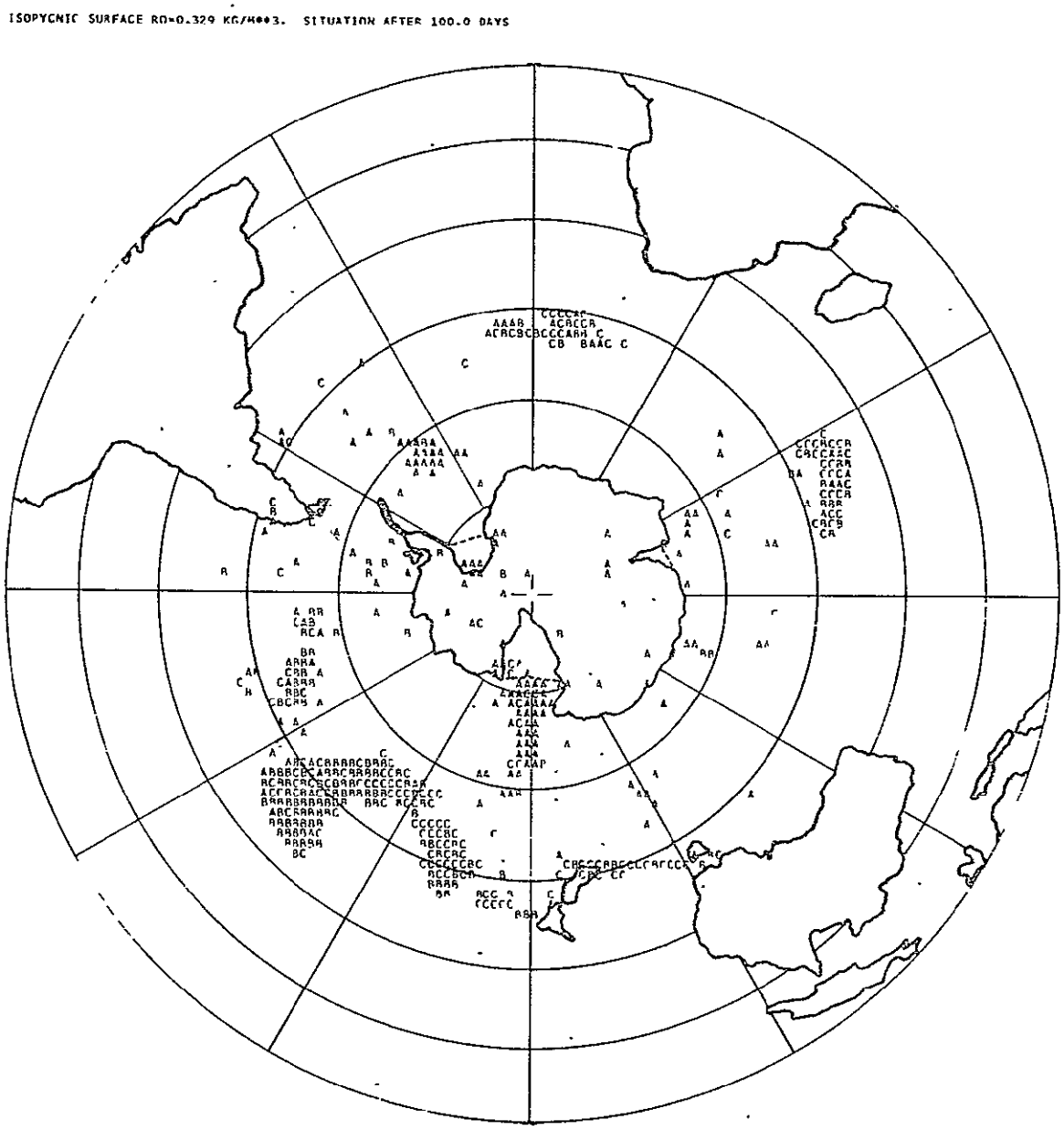

Fig. 22. Balloon positions, on a polar equal area projection, at day 100.

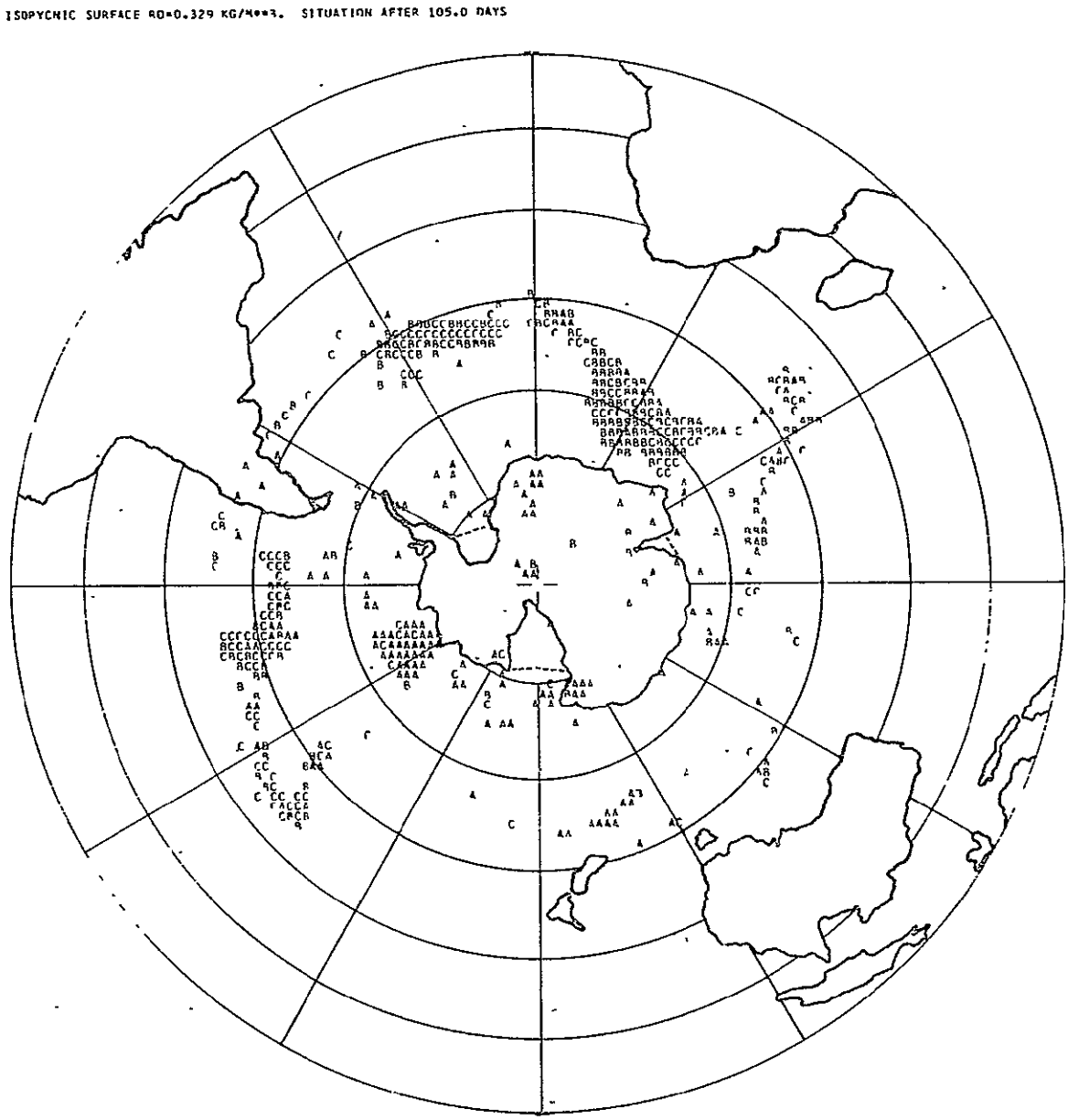

Fig. 23. Balloon positions, on a polar equal area projection, at day 105.

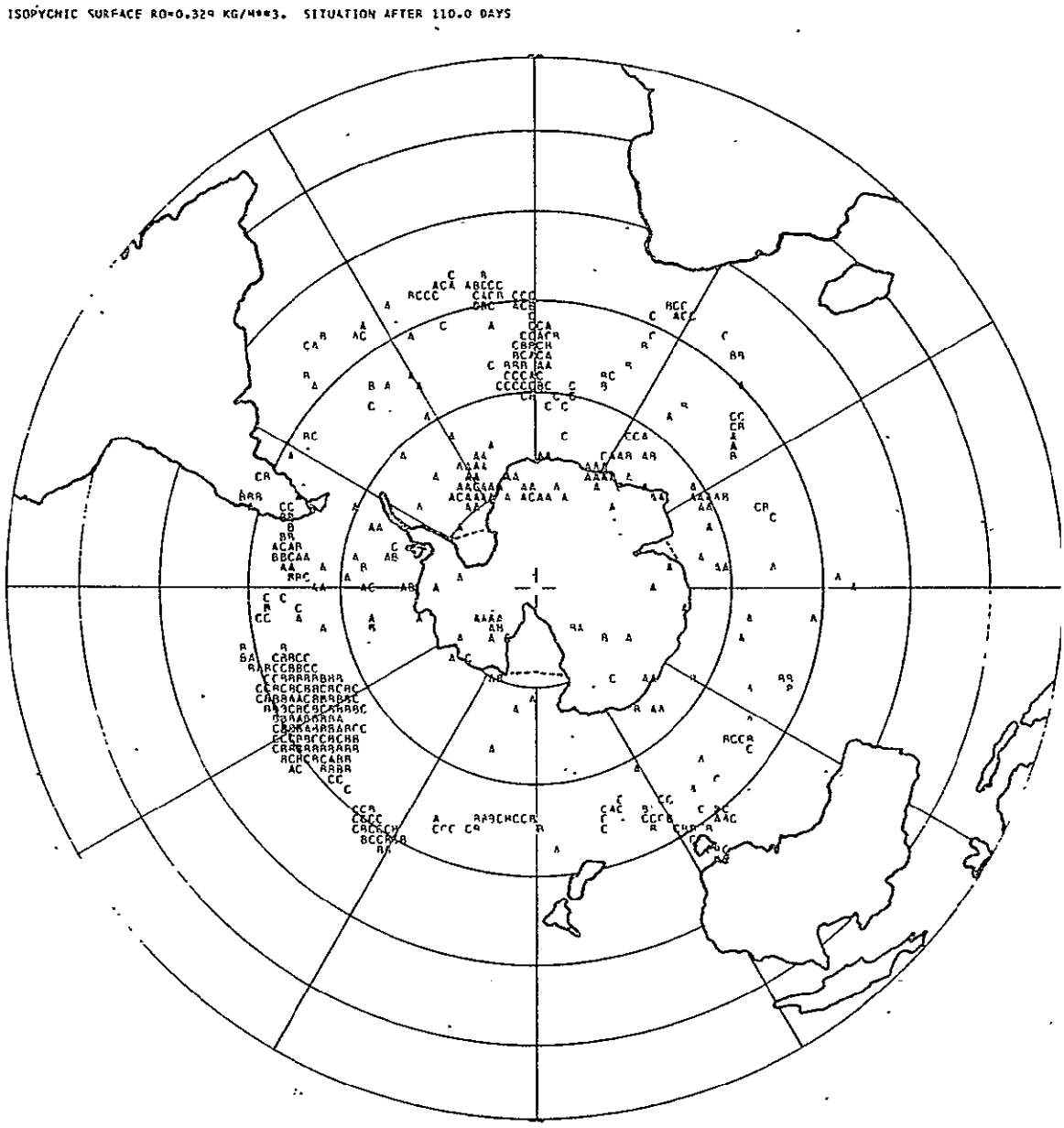

Fig. 24. Balloon positions, on a polar equal area projection, at day 110.

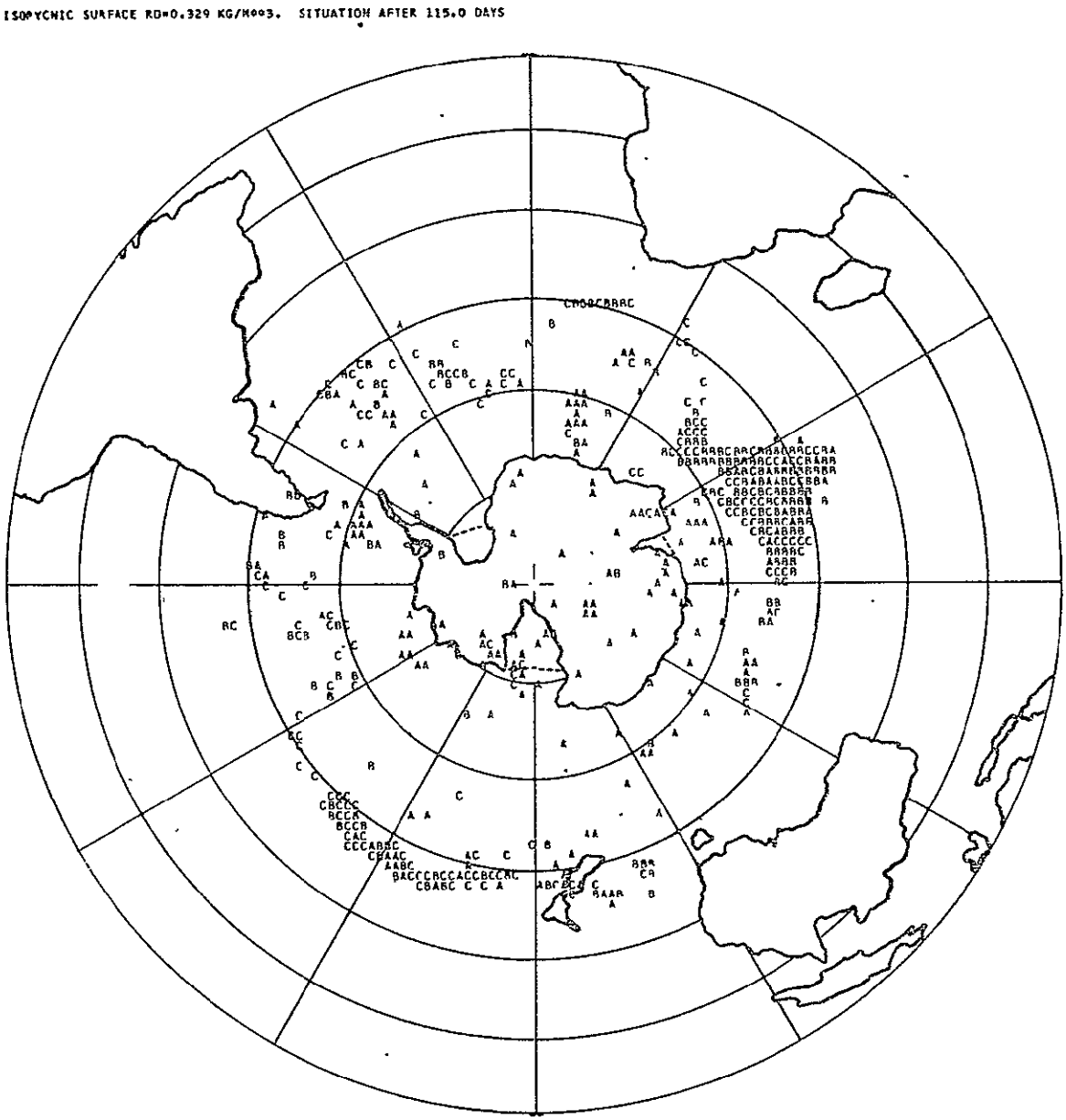

Fig. 25. Balloon positions, on a polar equal area projection, at day 115.

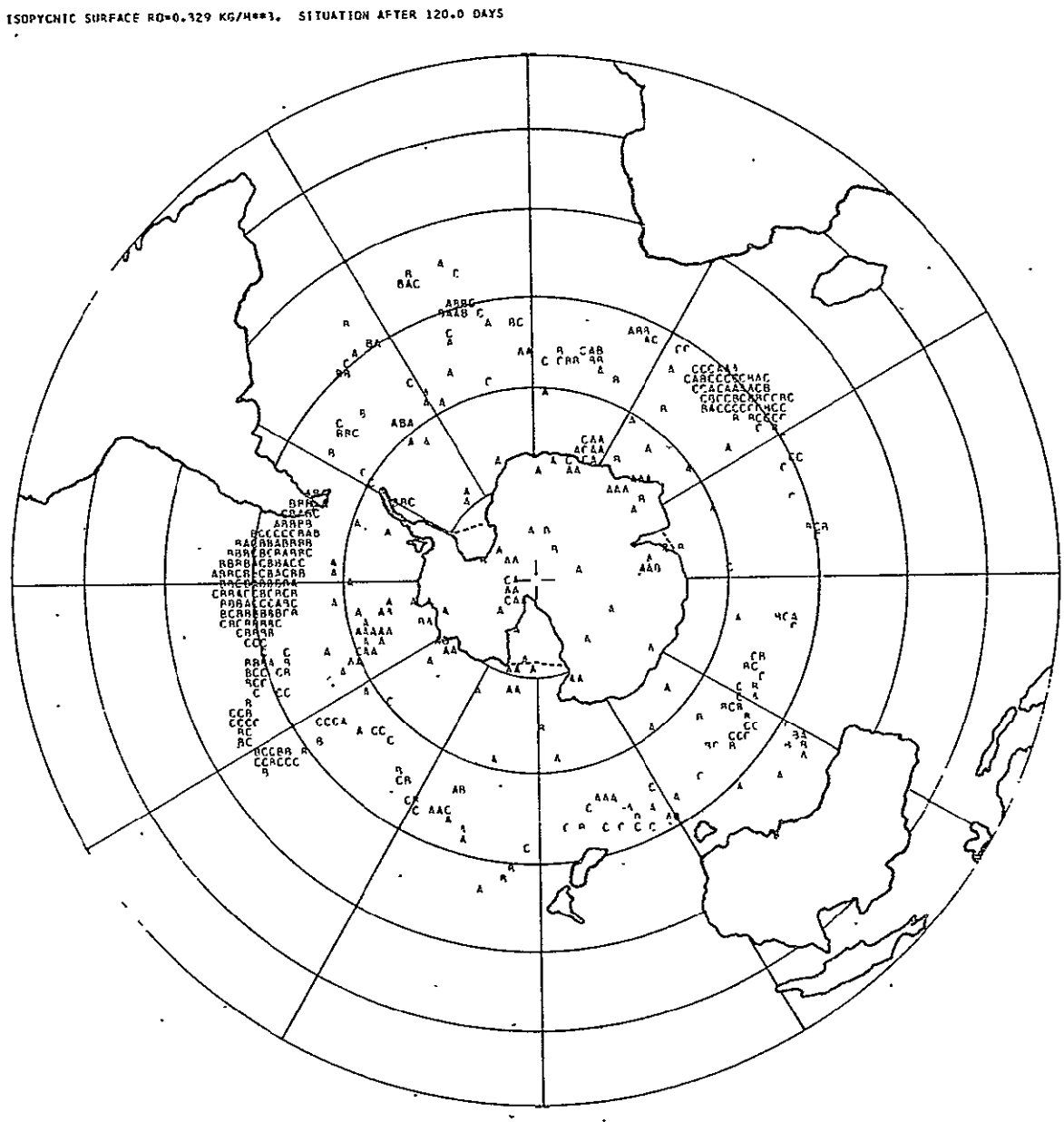

Fig. 26. Balloon positons, on a polar equal area projection, at day 120.

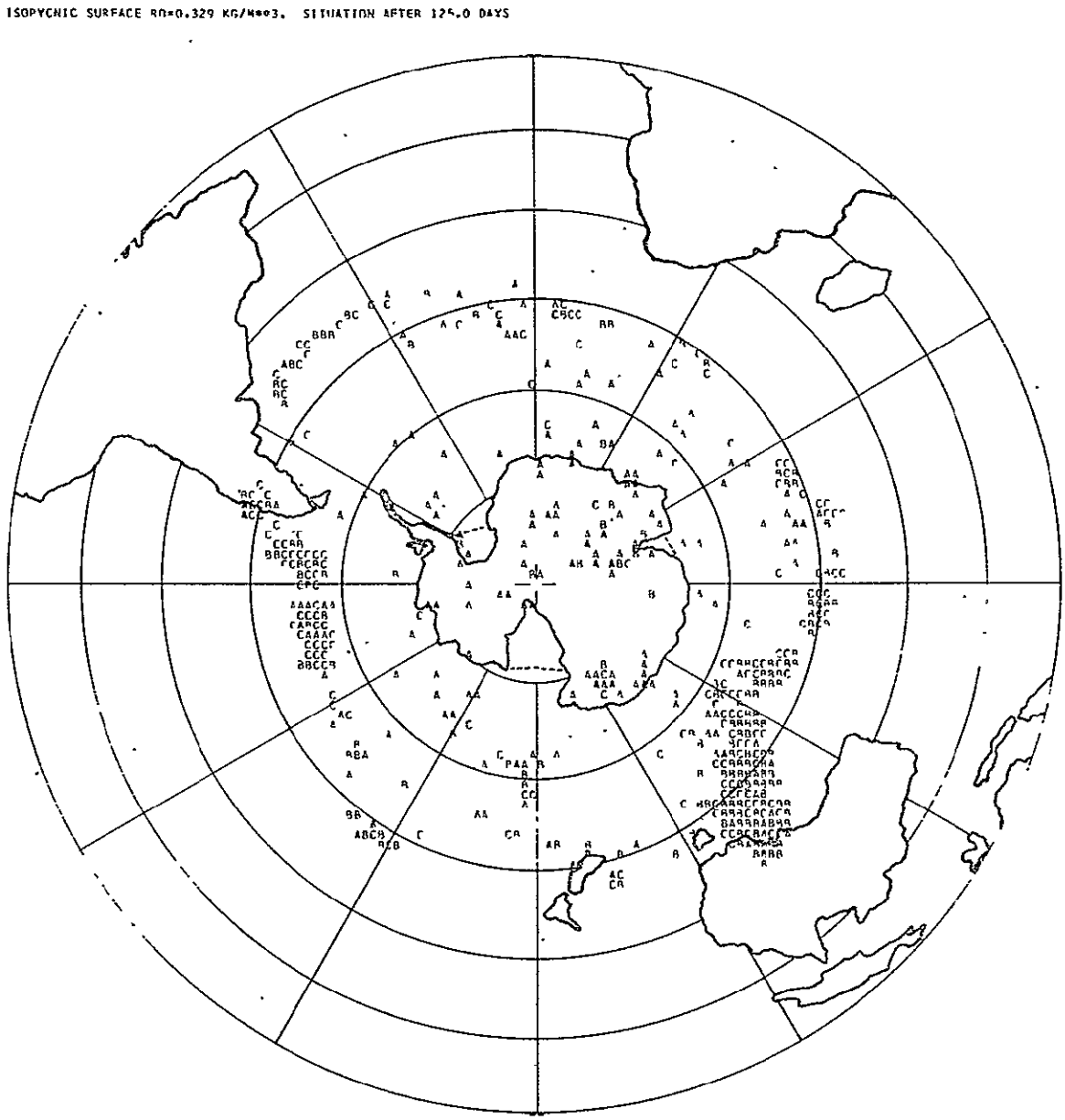

Fig. 27. Balloon positions, on a polar equal area projection, at day 125.

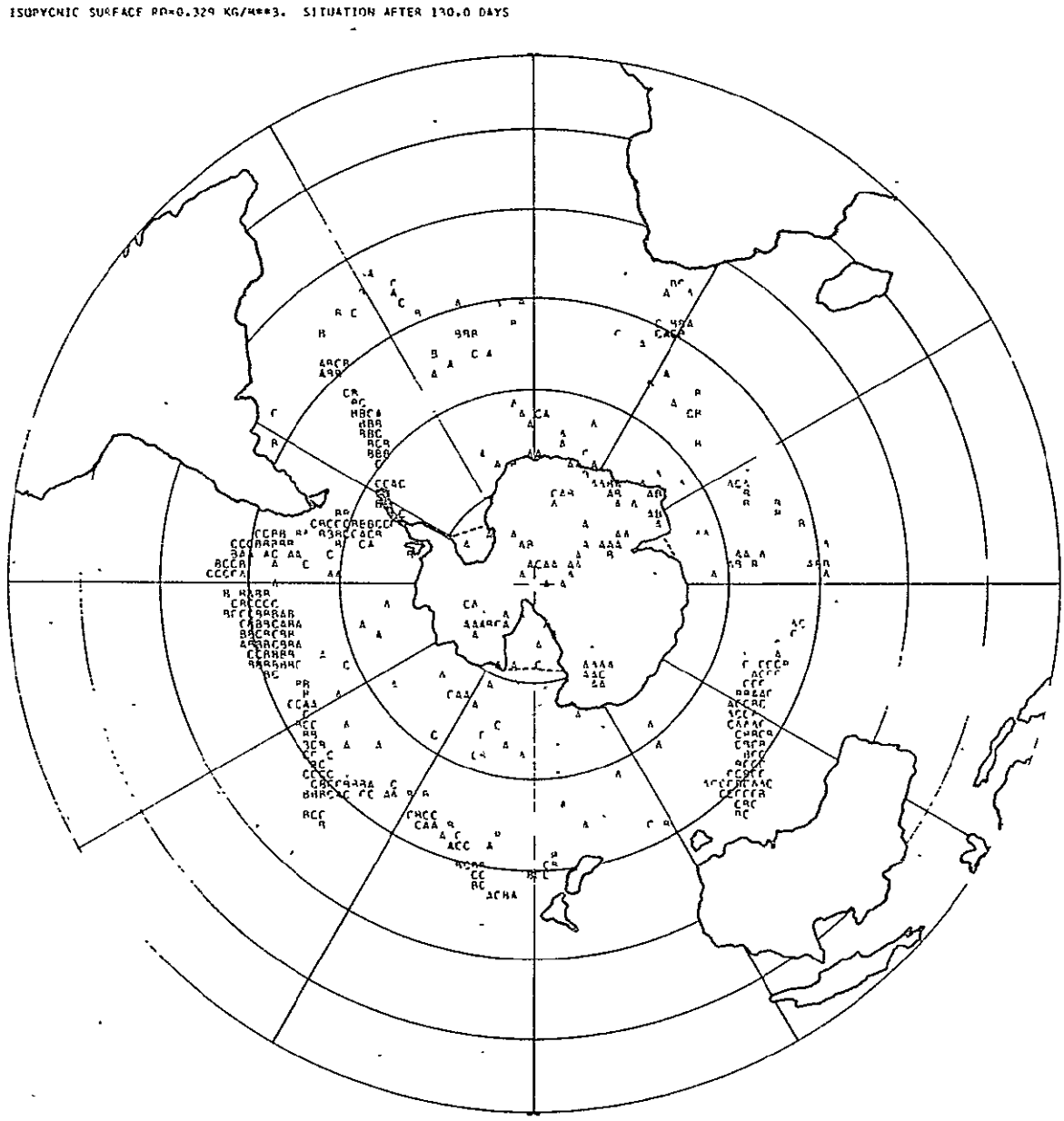

Fig. 28. Balloon positions, on a polar equal area projection, at day 130.

By about 30 days the balloons approach a quasi-steady state, in which almost all of the B and C balloons, and some of the A balloons, are within a band centered near 45°S latitude. Within this general zonal distribution there are several clusters. These clusters change in shape and intensity as they drift eastward with time, circling the globe in the order of ten days. The more intense and larger clusters can be traced on the consecutive 5 day maps.

From day 70 to day 80 a large cluster forms near the Ross Sea. It splits into two smaller clusters by day 90, and disperses almost completely by day 110.

From about day 85 to day 120 a single large cluster, near 45°S latitude, is very conspicuous in the balloon distribution. After day 120 it weakens by zonal elongation.

he gradual mixing of the three kinds of balloons can be followed on the consecutive maps; but it proceeds at a slow rate. Throughout the 130 days only a small number of the B and C balloons enter the central (polar) region. The central region remains mainly populated by the A balloons. On the other hand, a large fraction of the A balloons form part of the middle latitude zone of high density of balloons.

After day 25 (26 December, year 1), no balloons move northward across the 30°S latitude circle in the numerical simulation. After day 75 very few balloons move northward across 35°S latitude.

5. STATISTICAL DESCRIPTION OF THE BALLOON DISTRIBUTIONS

Two types of statistical description were made of the space-time distributions of the balloons in this simulation of the 1970-71 Eole Experiment.

In the first description, the degree of clustering is shown by taking 1000 points, located at random on the spherical earth poleward of 30°S latitude, and computing the average of the distance from each of these points to the nearest balloon. It was shown by Mesinger (1965) that if the balloons are randomly distributed with respect to each other, this average nearest balloon distance has a minimum value when the balloons have a constant density in space (a constant number per unit are). This minimum value is 0.5 when the unit of length is chosen to make the average density of balloons equal to 1 per unit area. (In the present study, when all 500 balloons are poleward of 30° latitude this unit of length is 505 kilometers; and the average nearest balloon distance, for balloons that are randomly distributed with a constant number per unit area, is 252.5 kilometers.) If the balloons deviate from the desired state of random distribution with a constant number per unit area, then the mean nearest balloon distance will be larger than 0.5; and its deviation from 0.5 will indicate the degree of balloon clustering.

Figure 29 shows the average nearest balloon distance as a function of time, as computed at 2.5 day intervals; starting from day 17.5, when all 500 balloons are in the air.

At day 17.5 the nearest balloon distance is 0.83 (approximately 420 km). It slowly increases with time to its maximum of 1.30 (657 km) at day 105.

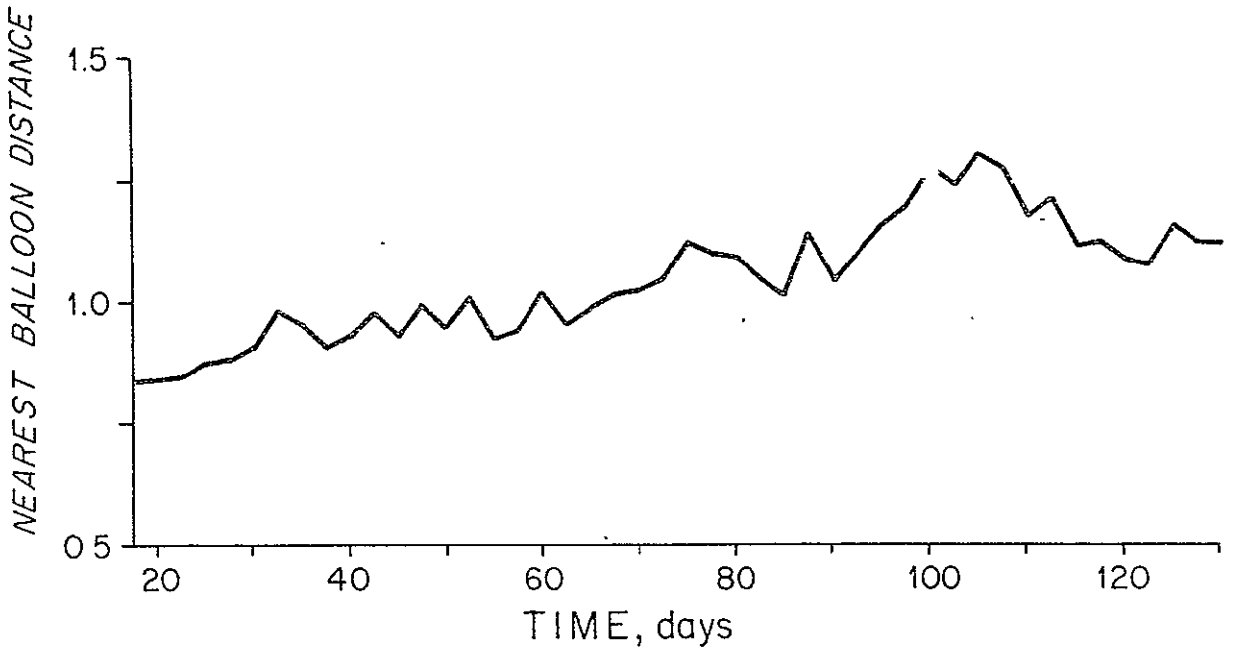

Fig. 29. Average distance to the nearest balloon from 1000 points located at random poleward of 30°S latitude (at intervals of 2.5 days). The unit of length is chosen to make the average density of balloons (the number per unit area), in the region poleward of 30°S, equal to 1. (When 500 balloons are poleward of 30°S, this unit of length is 505 kilometers.)

If we compare the map for day 105 (figure 23) with, say, the map for day 20 (figure 6), we see that on day 105 there are several strong clusters of balloons and also large empty areas near the 30° latitude limit. These strong clusters accompanied by large empty areas are not pronounced on the map for day 20. Day 85 has the smallest average nearest balloon distance during the last part of the simulation. The map for day 85 (figure 19) shows a smaller number of clusters than day 105 and smaller empty areas near the 30° latitude limit used in calculating this index.

In the second description of the balloon distributions, in figure 30, we show the distribution of the balloons with latitude, as averaged for the last 50 days of the simulation (day 80 to day 130). The last 50 days were chosen because the time-variation, shown in figure 29, indicates that the balloon distribution may already be in a statistically steady state. Figure 30 shows the average of 21 histograms, taken at 2.5 day intervals, in each of which the average density of balloons is computed for 5° latitude intervals. The ordinate scale on the left shows the density of balloons (the number per unit area) when the unit length is chosen such that the average density over the entire globe is 1. The ordinate scale on the right corresponds to the scale used in figure 29, where the unit length was chosen such that the average density over the polar cap south of 30°S latitude is equal to in which case the unit length is 505 km. The abscissa scale in figure 30 is proportional to the sine of the latitude.

Figure 30 shows that there is more than one balloon per $(505 \text{ km})^2$ in the latitude zone between 40°S and 55°S; and more than two balloons per $(505 \text{ km})^2$ in the zone 45°S to 50°S. There is a secondary maximum in the polar region, south of 75°S latitude. From 40°S to 35°S there is an average density of about 0.5 balloons per $(505 \text{ km})^2$. There were only three occasions (in the 21 histograms) in which a single balloon was between 35°S and 30°S. As inciated earlier, in none of these 21 histograms was there a balloon equatorward of 30°S latitude.

The distribution shown in figure 30 is based on a large number ($500 \times 21 = 10{,}500$) of balloon locations. The two maxima of balloon density, and the absence of balloons equatorward of 30°S latitude indicate the upper tropospheric convergence and divergence of the three cell mean meridional circulation produced in the numerical simulation of the global circulation.

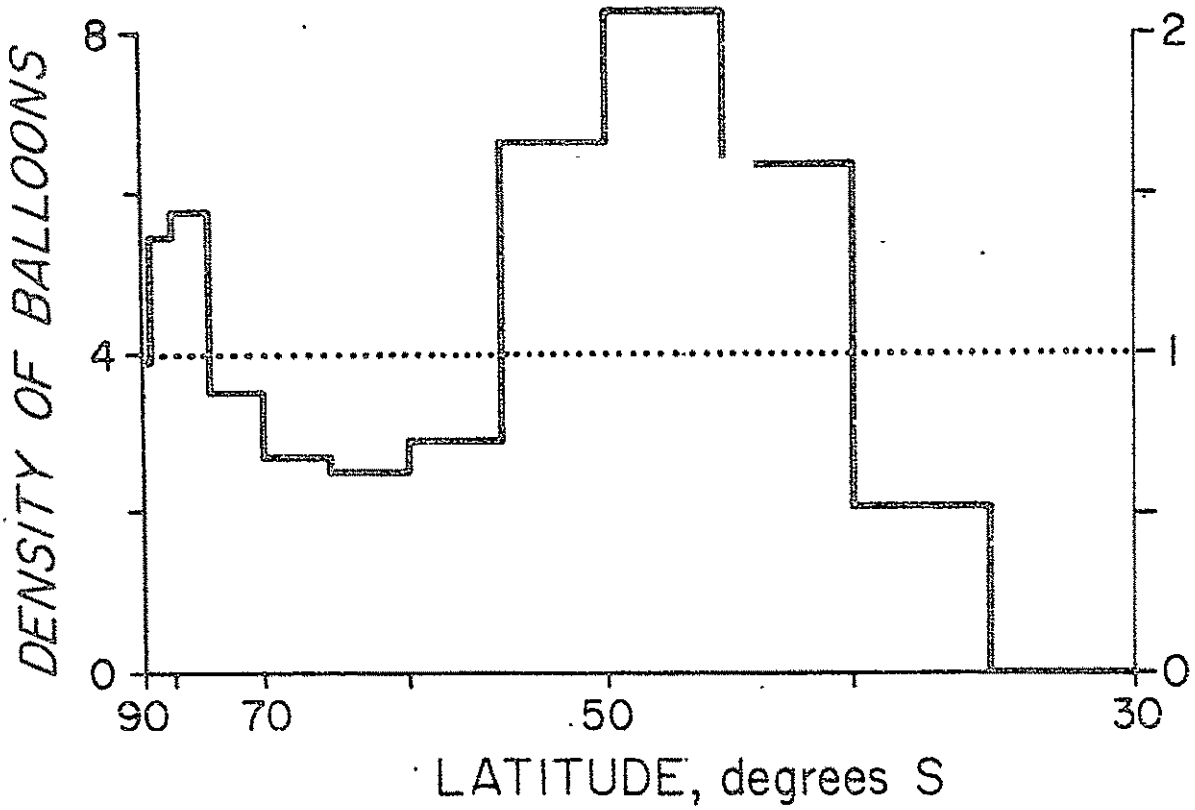

Fig. 30. The average density of balloons (the number per unit area) in each five degree latitude zone, averaged for the last 50 days of the numerical simulation. The abscissa scale is proportional to the sine of the latitude. The ordinate scale on the left gives the density of balloons when the unit of length is chosen such that the average density over the entire globe is 1. The ordinate scale on the right shows the number of balloons per $(505\ km)^2$. The dotted line represents the density when all the balloons are uniformly distributed poleward of 30^oS latitude.

As indicated earlier, figures 1 through 28 show that very few of the B and C balloons (those released at Neuquén and Mendoza) enter the polar region; whereas a large fraction of the A balloons (those released at Lago Fagnano) move into middle latitudes. This suggests that we should examine the space-time distribution of just the A balloons by themselves.

In figure 31, the solid curve is from figure 29, and is based on all 500 A, B and C balloons. The dashed curve is the same statistical representation based only upon the 167 A balloons (the Lago Fagnano balloons). From about day 30 on, the average of the nearest balloon distance, for the A balloons alone, is closer to the value for a random balloon distribution (0.5), than is the curve for the balloons from all three launch sites. This, of course, is only the statistical statement of what the maps showed.

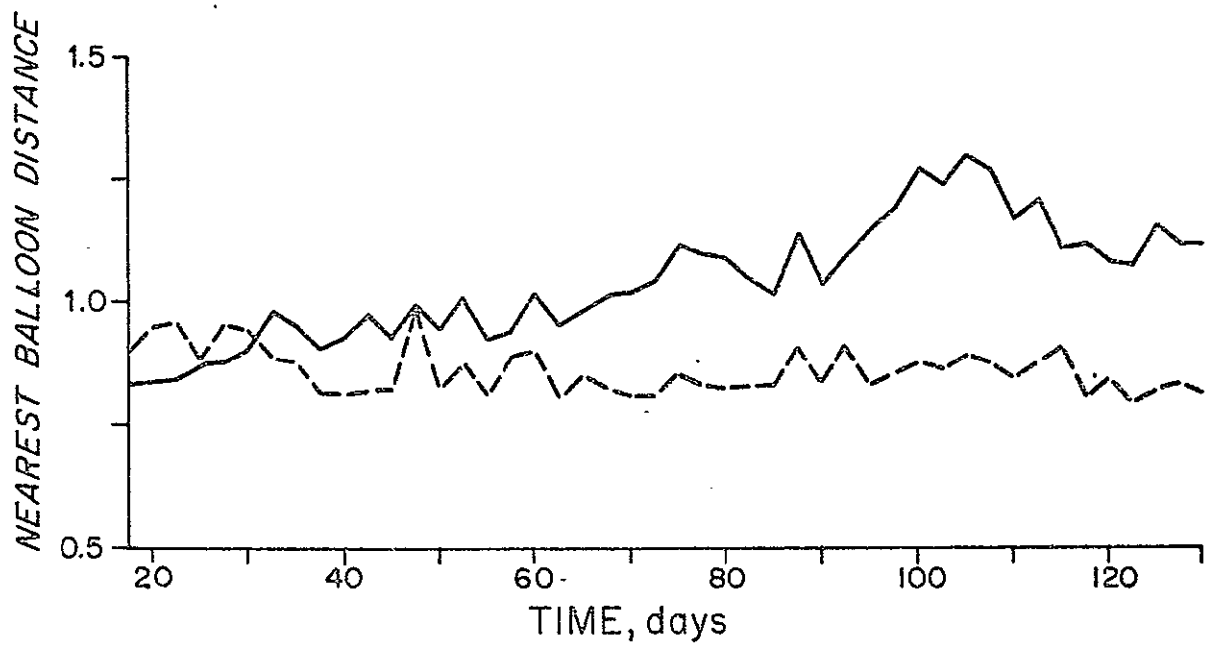

Fig. 31. Average distance to the nearest balloon from 1000 points located at random poleward of 30°S latitude (at intervals of 2.5 days). The unit of length is chosen to make the average density of balloons (the number per unit area), in the region poleward of 30°S, equal to 1. The solid curve is the distribution shown in figure 29, based on balloons A, B and C. The dashed curve is the distribution obtained with only the 167 A balloons (those released at Lago Fagnano).

In figure 32, the solid curve is from figure 30, and is based on all 500 A, B and C balloons. The dashed curve is the same statistical representation for the 167 A balloons only. The more pronounced polar maximum of the A balloons alone, reflects the fact that relatively few B and C balloons entered this region. From 70°S to 45°S the distribution of the A balloons is more uniform with latitude than the distribution which included the B and C balloons. But between 40°S and 35°S the density of the A balloons alone is poorer than the density for the A, B and C balloons.

6. TEST COMPARISON WITH OBSERVED GHOST BALLOONS

To evaluate the reliability of the results given above, we made a test comparison with observed GHOST balloon trajectories.

Solot (1968) showed the trajectories of 9 balloons at the density surface ρ_2 (for 200 mb). Of these, 7 balloons were in the air during the 100 day period 1 January to 11 April 1967. All the GHOST balloon data for this 100 day period was used in our test comparison. Table I shows the time period and initial location of the GHOST balloons.

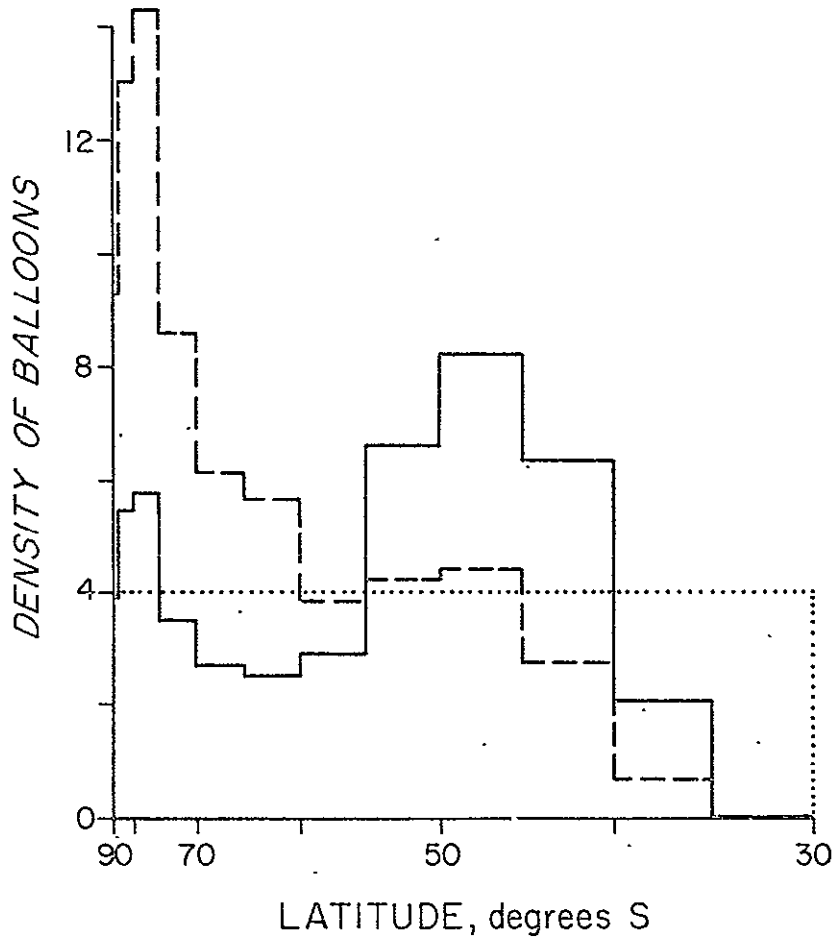

Fig. 32. The average density of balloons (the number per unit area) in each five degree latitude zone, averaged for the last 50 days of the numerical simulation experiment. The abscissa scale and the left side ordinate scale are the same as in figure 30. The solid curve is the distribution shown in figure 30, based on balloons A, B and C. The dashed curve is the distribution obtained with only the 167 A balloons (those released at Lago Fagnano). The dotted line represents the density of balloons when they are all uniformly distributed poleward of 30°S latitude.

TABLE I

GHOST BALLOONS (Data from Solot, 1968)

Balloon Letter	NCAR Identification	Period	Initial Location
A	49R	1 Jan - 12 Jan	31.55°S, 124.71°W
B	34J	1 Jan - 13 Jan	46.43°S, 134.91°E
C	50D	1 Jan - 1 Feb	64.03°S, 44.72°W
D	58G	1 Jan - 25 Feb	53.21°S, 62.20°E
E	60TA	1 Jan - 11 April	59.40°S, 46.12°W
F	70K	19 Jan - 11 April	55.94°S, 160.41°W
G	79R	17 Feb - 11 April	45.97°S, 148.77°W

There were 5 GHOST balloons in the air on January 1st, 1967. Their 0.0 GMT positions on 1 January are therefore taken as the initial locations for this study. Two balloons were launched later, and their first locations are given by Solot for 19 January and 17 February respectively. Only balloons E, F and G remained in the air until the end of our 100 day test period. During the 100 day test period there were never less than three nor more than five GHOST balloons in the air at any one time.

Taking the once per day (0.0 GMT) position of each of these GHOST balloons, we obtain a total of 351 positions, which are shown in figure 33. This gives an average of 3.5 balloon positions per day.

At each intitial location and initial time of the 7 GHOST balloons, shown in table I, we introduced into the numerical simulation of the global atmospheric circulation, at ρ_2 (for 200 mb), a simulated GHOST balloon, each of which was allowed to stay in the air for the same period as the corresponding true GHOST balloon. The once per day (0.0 GMT) positions of the simulated balloons, which also total 351 positions, are shown in figure 34.

It is important to stress two factors when comparing the true and the simulated GHOST balloon positions. The first is that the year of the true GHOST balloon trajectories is year 1967 AD, whereas the year of the simulated GHOST balloon trajectories in the year 2 in the numerical simulation of the atmosphere. Only the initial calendar day, and the initial location on that day, were the same for each balloon, A through G.

The second important factor, in the test comparison, is that the number of balloons, never more than 5 at any one time, is a very small sample.

Comparing figures 33 and 34 we are impressed by their similarity. In both cases the balloons are uniformly distributed in the region poleward of 45°S latitude, with a rapid decrease of balloon density equatorward of that latitude.

In this time-space representation, a cluster is produced if a weak wind allows a single balloon to stagnate in a given region. But in the preceding space representations, figures 1 through 28, clustering was produced when different balloons were brought together by the convergent component of the wind field.

Figure 35 shows histograms for the 351 locations shown in the maps of figures 33 and 34. We notice the absence of the middle latitude maximum that was seen in figure 30. By comparing the maps of days 30 to 80 (figures 8 to 18) with the maps of days 80 to 130 (figures 18 to 28), we see that the difference in histograms cannot be accounted for by any difference of the circulation regime between the first half and the second half of the 100 day period used to obtain the lower histogram in figure 35. Therefore, the difference in histograms must be due to the insufficient size of the GHOST defined sample. The small sample also explains the large magnitude of the polar maximum in the simulated GHOST distribution. This maximum is produced by a single balloon (balloon E) stagnating in the zone between 70° and 80°S latitude.

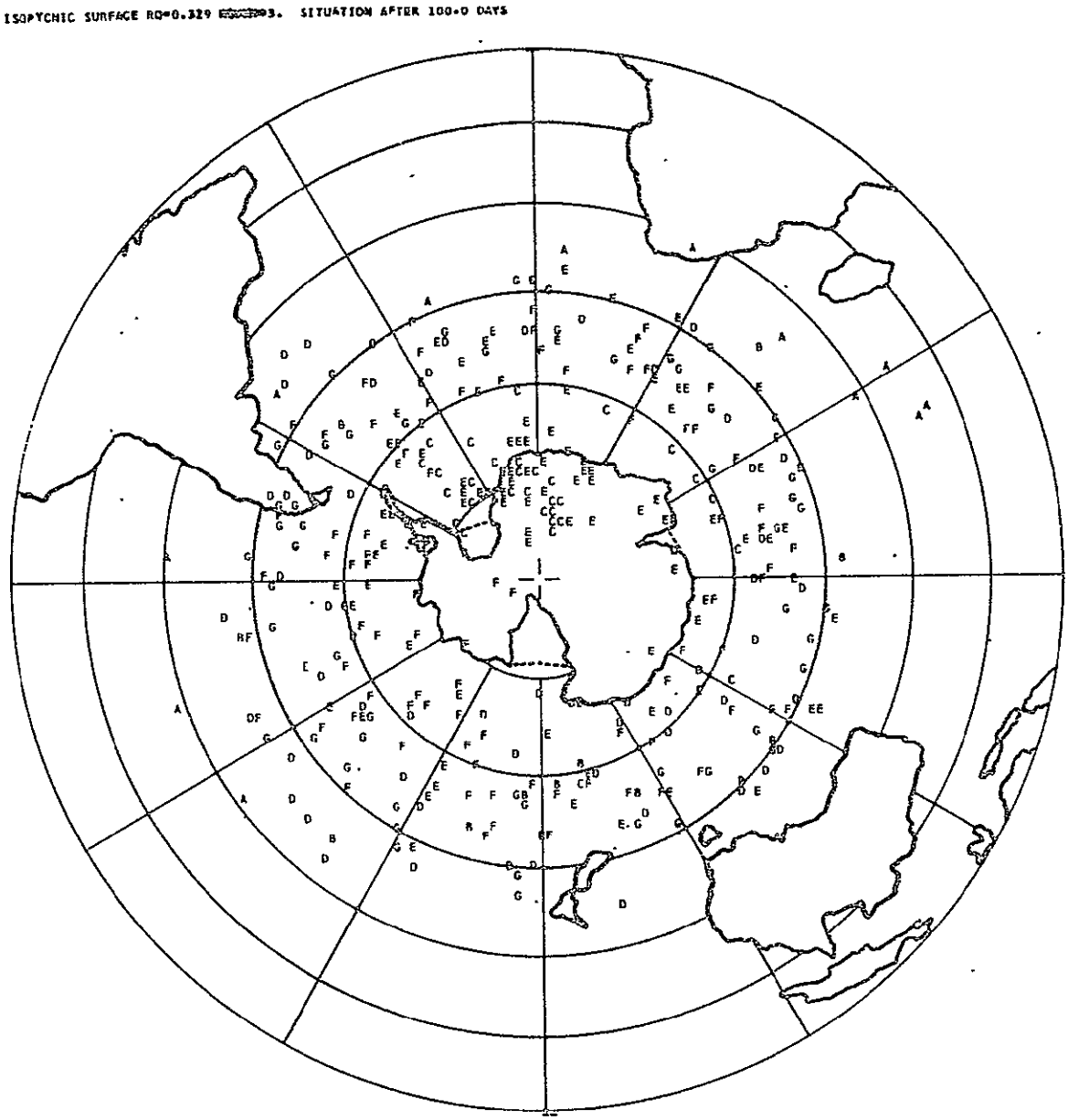

Fig. 33. Once a day positions, on an equal area projection, of all the observed GHOST balloons which were in the air during the first 100 days of 1967. (See table I and text for identification of the balloons A through G.)

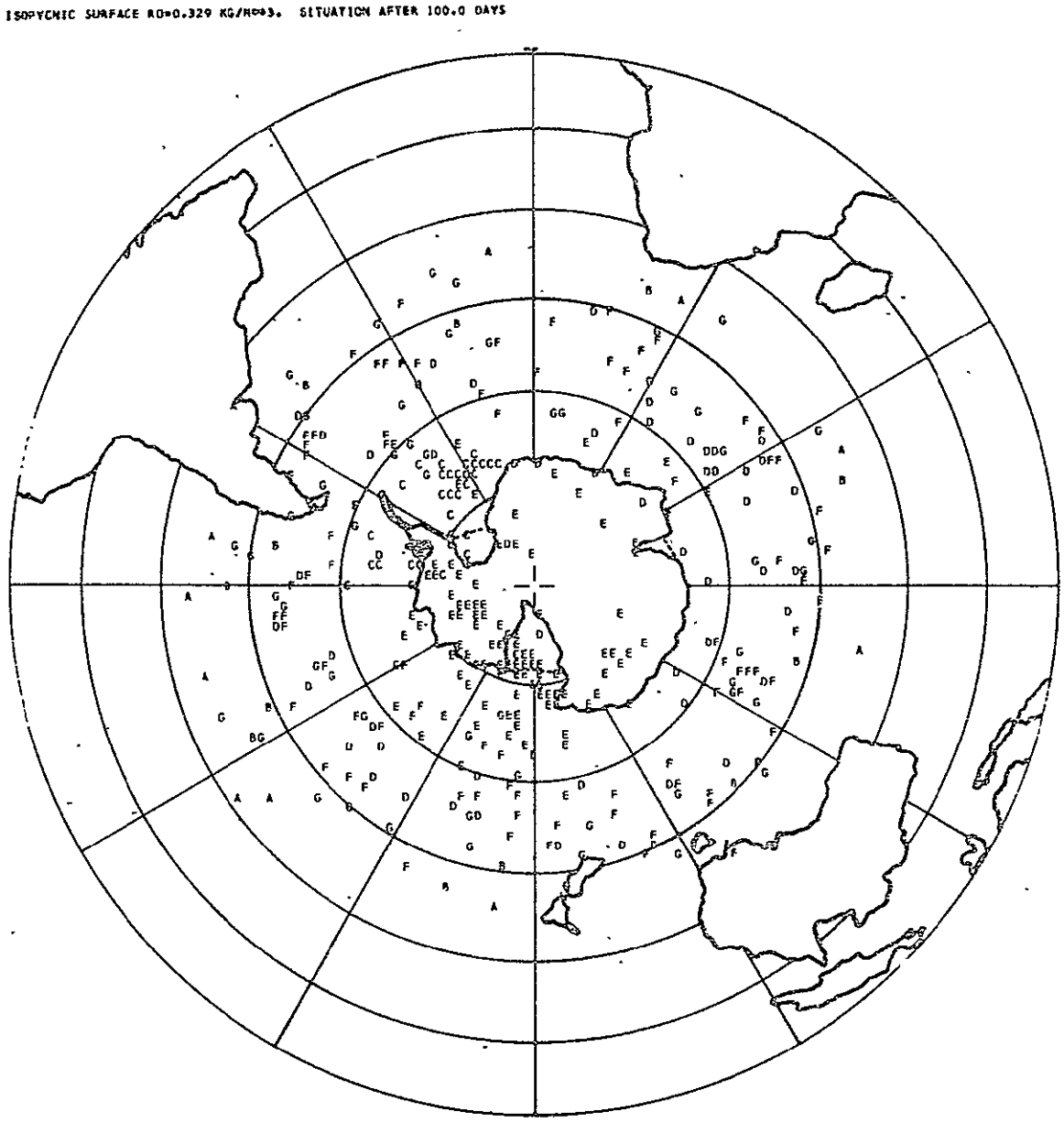

Fig. 34. Once a day positions, on an equal area projection, of the simulated GHOST balloons, A through G, for the first 100 days of year 2 in the numerical simulation.

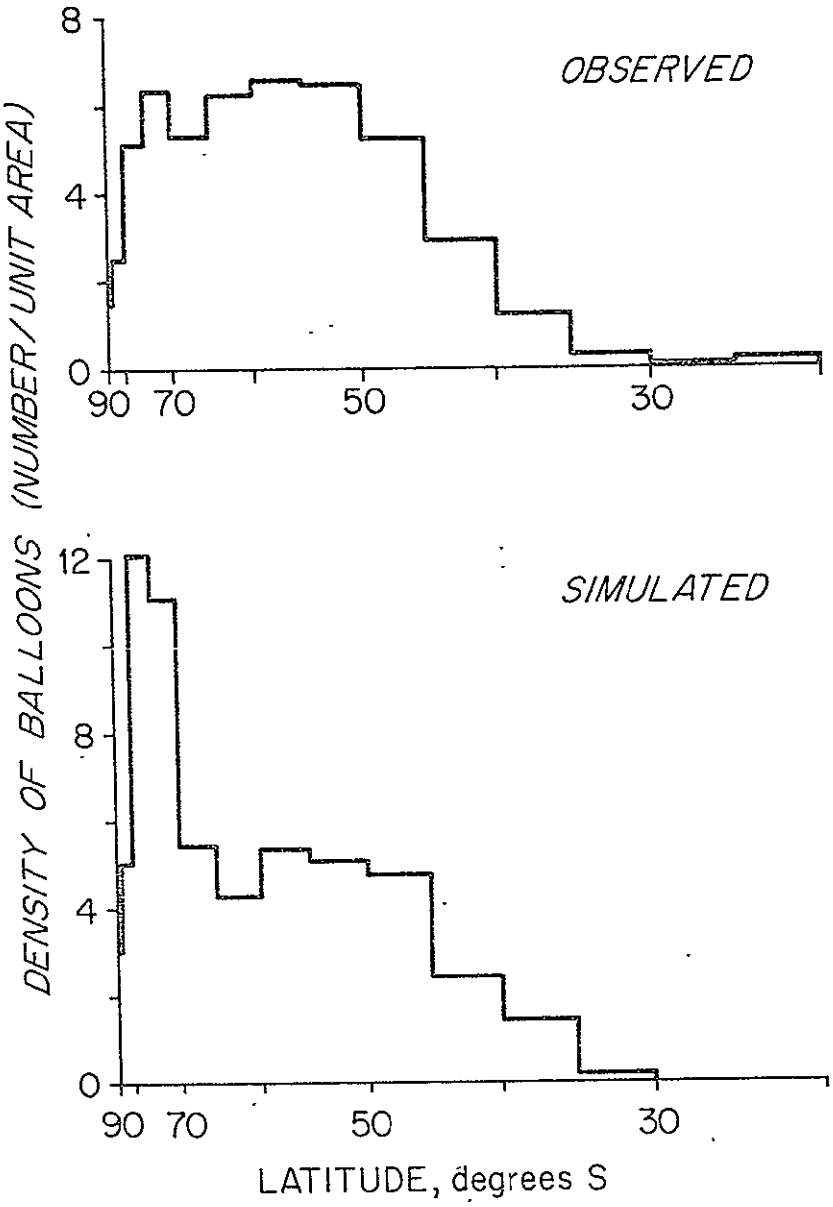

Fig. 35. Observed and simulated average density of the GHOST balloons (the number per unit area) in each five degree latitude zone, computed from the balloon positions shown in figures 33 and 34. The ordinate scale is the same as on the left side of figure 30.

On the other hand, we see in figure 33 and in figure 35 that one of the true GHOST balloons was in the latitude zone 30° to 20°S on four days; but that this was not the case for any of the simulated GHOST balloons. Although year 1967 and year 2 constitute a very small sample of years, this discrepancy may indicate a true, though small, difference between the real atmosphere and the numerically simulated atmosphere (in the sense that the real atmosphere may have a somewhat smaller constraint on the migration of balloons into the upper troposphere tropics).

On the whole, the overall similarity between the observed and simulated GHOST balloon distributions in this test comparison is close enough to make us believe that the space-time distributions of the large number of balloons in the planned 1970-71 Eole Experiment will be approximately the same as the simulated distributions shown in sections 4 and 5 above.

7. SUMMARY AND CONCLUSIONS

In our numerical simulation of the Eole Experiment, nearly all of the balloons end up in the region poleward of 35°S latitude, with a distribution in which the average distance from random points to the nearest balloon is about twice as large as it would be if the balloons were distributed at random within that region.

In the numerical simulation, there is a maximum density of balloons in a zone near 45°S latitude, where the density is about twice the average value.

Within this zone, in turn, there are usually several clusters. These clusters change in shape and intensity as they move eastward around the globe, making one revolution in the order of 10 days. Another, but less intense maximum density of balloons is found in the polar region, where clusters occasionally form.

A test comparison, with the small sample of 7 observed GHOST balloons, indicates that in the real atmosphere of the Southern Hemisphere summer the balloons move closer to the equator than in the simulation experiment. But in all other aspects the test comparison indicates a high reliability of the numerical simulation.

The fact that very few of the balloons launched at Mendoza and Neuquén enter the polar region, whereas the balloons launched at Lago Fagnano not only are well dispersed within the polar region but also have a fairly good latitudinal distribution in the middle latitudes, suggests that, with these particular launching sites, one would obtain a better (more homogeneous) space distribution of the balloons by launching more than one third of the total number of balloons at Lago Fagnano.

8. ACKNOWLEDGMENTS

The research reported here was done with the support of NASA Grant No. NGR 05 007 091.

The wind and mass fields used to simulate the constant-volume balloon trajectories were taken from a research project on Numerical Simulation of the General Circulation of the Atmosphere, which was supported by the Atmospheric Sciences Section, National Science Foundation, NSF Grant GA-1470.

REFERENCES

Arakawa, A., Mintz, Y. and Katayama, A., 1970: A Model for Numerical Simulation of the General Atmospheric Circulation and Global Climate. (in preparation)

Henrici, P., 1962: Discrete Variable Methods in Ordinary Differential Equations. New York, Wiley, 408 pp.

WMO-ICSU Joint Organizing Committee, 1969: The planning of the First GARP Global Experiment. World Meteorological Organization, Geneva. GARP Publications Series, No. 3, 36 pp.

Lally, V. E. and Lichfield, E. W., 1969: Summary of Status and Plans for the GHOST Balloon Project. Bull. Amer. Meteor. Soc., Vol. 50, pp. 867-874.

Mesinger, F., 1965: Behavior of a Very Large Number of Constant-Volume Trajectories. J. Atmos. Sci., Vol. 22, pp. 479-492.

Morel, P., 1969: Constant Level Balloon Flights Program in France. Laboratoire de Meteorologie Dynamique, Centre National de la Recherche Scientifique France. Report No. 6, 37 pp.

Solot, S. B., 1968: GHOST Balloon Data, Vols. 1-11. National Center for Atmospheric Research, Boulder, Colo., Technical Note No. 34.